THE UNIVERSITY of EDINBURGH

Edinburgh Research Explorer

# Molecular noise induces concentration oscillations in chemical systems with stable node steady states

**Citation for published version:**
Toner, DLK & Grima, R 2013, 'Molecular noise induces concentration oscillations in chemical systems with stable node steady states', *The Journal of Chemical Physics*, vol. 138, no. 5, 055101. https://doi.org/10.1063/1.4788979

**Digital Object Identifier (DOI):**
10.1063/1.4788979

**Link:**
Link to publication record in Edinburgh Research Explorer

**Document Version:**
Publisher's PDF, also known as Version of record

**Published In:**
The Journal of Chemical Physics

**General rights**
Copyright for the publications made accessible via the Edinburgh Research Explorer is retained by the author(s) and / or other copyright owners and it is a condition of accessing these publications that users recognise and abide by the legal requirements associated with these rights.

**Take down policy**
The University of Edinburgh has made every reasonable effort to ensure that Edinburgh Research Explorer content complies with UK legislation. If you believe that the public display of this file breaches copyright please contact openaccess@ed.ac.uk providing details, and we will remove access to the work immediately and investigate your claim.

Download date: 04. May. 2023

The Journal of Chemical Physics

# Molecular noise induces concentration oscillations in chemical systems with stable node steady states

Cite as: J. Chem. Phys. **138**, 055101 (2013); https://doi.org/10.1063/1.4788979
Submitted: 20 October 2012 . Accepted: 09 January 2013 . Published Online: 04 February 2013

D. L. K. Toner, and R. Grima

View Online Export Citation CrossMark

ARTICLES YOU MAY BE INTERESTED IN

The chemical Langevin equation
The Journal of Chemical Physics **113**, 297 (2000); https://doi.org/10.1063/1.481811

Steady-state fluctuations of a genetic feedback loop: An exact solution
The Journal of Chemical Physics **137**, 035104 (2012); https://doi.org/10.1063/1.4736721

How accurate are the nonlinear chemical Fokker-Planck and chemical Langevin equations?
The Journal of Chemical Physics **135**, 084103 (2011); https://doi.org/10.1063/1.3625958

Lock-in Amplifiers up to 600 MHz
Watch

AIP Publishing



© 2013 American Institute of Physics.

# Molecular noise induces concentration oscillations in chemical systems with stable node steady states

D. L. K. Toner and R. Grima
*SynthSys Edinburgh, School of Biological Sciences, University of Edinburgh, Edinburgh EH9 3JR, United Kingdom*

(Received 20 October 2012; accepted 9 January 2013; published online 4 February 2013)

It is well known that internal or molecular noise induces concentration oscillations in chemical systems whose deterministic models exhibit damped oscillations. In this article we show, using the linear-noise approximation of the chemical master equation, that noise can also induce oscillations in systems whose deterministic descriptions admit no damped oscillations, i.e., systems with a stable node. This non-intuitive phenomenon is remarkable since, unlike noise-induced oscillations in systems with damped deterministic oscillations, it cannot be explained by noise excitation of the deterministic resonant frequency of the system. We here prove the following general properties of stable-node noise-induced oscillations for systems with two species: (i) the upper bound of their frequency is given by the geometric mean of the real eigenvalues of the Jacobian of the system, (ii) the upper bound of the Q-factor of the oscillations is inversely proportional to the distance between the real eigenvalues of the Jacobian, and (iii) these oscillations are not necessarily exhibited by all interacting chemical species in the system. The existence and properties of stable-node oscillations are verified by stochastic simulations of the Brusselator, a cascade Brusselator reaction system, and two other simple chemical systems involving auto-catalysis and trimerization. It is also shown how external noise induces stable node oscillations with different properties than those stimulated by internal noise. © *2013 American Institute of Physics*. [http://dx.doi.org/10.1063/1.4788979]

## I. INTRODUCTION

Concentration oscillations are a ubiquitous characteristic of intracellular dynamics.[1] The period of these oscillations can vary from few seconds to several hours, well-known examples being calcium oscillations (seconds to minutes),[2] glycolytic oscillations (minutes),[3] and circadian rhythms (1 day).[4]

The oscillatory properties of various biochemical circuits have been extensively studied by means of the rate equation formalism.[5] This deterministic framework allows one to build time evolution equations for the concentrations, the rate laws being determined by the principle of mass action. A common strategy to analyze these equations is linear stability analysis by which one derives an equation for the time evolution of a small perturbation about the steady state of the system. From this analysis one can determine, by consideration of the eigenvalues of the Jacobian of the rate equations, if these small perturbations will decay in a non-oscillatory manner (a stable node), decay in an oscillatory manner (a stable focus) or lead to periodic oscillations (a limit cycle). The last case is that in which the steady state loses stability and is replaced by sustained oscillations, conditions which are achieved when the system possesses a negative feedback mechanism with sufficient memory, sufficient nonlinearity in the reaction rates, and a proper balancing of the time scales of species involved in the feedback loop.[6] It has been shown that the minimal realistic chemical system, i.e., that composed of a set of unimolecular and bimolecular reactions, which satisfies these properties involves the interaction of three species.[7]

Deterministic approaches are valid in the limit of large molecule numbers. Contrastingly the number of molecules per cell of many intracellular chemical species is quite small (few tens to few thousands—see, for example Ref. 8). In such conditions the stochasticity in reaction kinetics cannot be ignored.[9] These fluctuations are an inherent property of the system and cannot be turned off; they are commonly referred to as internal or intrinsic noise. Thus deterministic approaches may not lead to an accurate description of many intracellular biochemical oscillators.

Stochastic models of biochemical oscillators have thus become more common in the past decade,[10–13] their dynamics being explored principally by means of the stochastic simulation algorithm.[14] To a lesser extent, the problem has also received theoretical attention by analysis of the chemical master equation,[15] a set of differential-difference equations containing complete information about the stochastic properties of the trajectories generated by the stochastic simulation algorithm. This led to the important insight that stochasticity is not necessarily detrimental to the production of sustained oscillations but that rather it can promote oscillations. In particular, using the linear-noise approximation[15] of the chemical master equation, it was shown that internal noise induces sustained oscillations in biochemical networks whose deterministic rate equations predict stable foci, i.e., those whose perturbations decay in an oscillatory manner.[16,17] The intuitive reason for this phenomenon is that the "underlying stochasticity has a flat spectrum in frequency space (i.e., white noise), and this automatically excites the resonant frequencies of the system,"[16] i.e., the frequency of the damped oscillations in

 © 2013 American Institute of Physics

the deterministic model. Similar conclusions were reached by means of multiple-scale analysis in the context of oscillating numbers of infected individuals in a population[18] and by analysis of the Q-matrix in simple models of biochemical reactions.[19]

In this article, we show that internal noise induces oscillations even in biochemical systems whose deterministic rate equation models predict a stable node. This is remarkable since it cannot be explained by the intuitive reasoning used for noise-induced oscillations (NIO) associated with stable foci. In particular, stable nodes are not characterized by a damped oscillatory return to steady state and hence there does not exist a resonant frequency which white noise can excite. We also show that external noise (noise whose origin lies outside the chemical system under consideration[20]) can as well lead to NIO in stable node systems, albeit these having different properties than NIO produced by internal noise.

The article is divided as follows. In Sec. II we provide a short summary of the linear-noise approximation theory for NIO. In Sec. III we use this theory to show that NIO can be observed for systems with a stable node. General properties of these NIO such as their frequency and quality and the fundamental reason for their origin are studied in Sec. IV. The existence of these new types of NIO are verified by means of stochastic simulations of three simple chemical systems involving the interaction of two species in Sec. V. Therein we also study the relationship between the quality of the NIO and the distance from the node-focus borderline in phase space, as well as the robustness of the linear-noise approximation results for small molecule numbers. In Sec. VI we show that in some cases, the quality of stable node NIO improves dramatically with the number of interacting species thus lending evidence of their possible importance in large biochemical networks. In Sec. VII we show that external noise generates stable node NIO with properties differing from those produced by internal noise. Finally, we conclude with a discussion in Sec. VIII.

## II. DESCRIPTION OF NIO USING THE LINEAR-NOISE APPROXIMATION

### A. Preliminaries

Consider a general reaction system containing $N$ distinct chemical species which react according to $R$ distinct reactions in a compartment of volume $\Omega$. A particular reaction $j$ can be written in the general form,

$$\sum_{i=1}^{N} s_{ij} X_i \xrightarrow{k_j} \sum_{i=1}^{N} r_{ij} X_i, \tag{1}$$

where the $s_{ij}$ and $r_{ij}$ are the stoichiometric coefficients. According to this formulation, if species $X_i$ is not involved in reaction $j$ as a reactant (product) then $s_{ij}$ ($r_{ij}$) is simply set to zero.

Assuming well-mixed conditions, the state of the system at any time $t$ is completely described by the vector of the number of molecules of each species, $\vec{n} = (n_1, n_2, \ldots, n_N)$. At random times, one of the $R$ reactions (say reaction $j$) occurs somewhere in the volume $\Omega$ and the state vector changes from some $(n_1, n_2, \ldots, n_N)$ to $(n_1 + S_{1j}, n_2 + S_{2j}, \ldots, n_N + S_{Nj})$ where $S_{ij} = r_{ij} - s_{ij}$. Realizations of this stochastic process can be obtained by the stochastic simulation algorithm. Alternatively, the statistical properties of the stochastic process are completely described by the chemical master equation:[15,21]

$$\frac{\partial P(\vec{n}, t)}{\partial t} = \Omega \sum_{j=1}^{R} \left( \prod_{i=1}^{N} E_i^{-S_{ij}} - 1 \right) \hat{f}_j(\vec{n}, \Omega)\ P(\vec{n}, t), \tag{2}$$

where $P(\vec{n}, t)$ is the probability of the system being in state $\vec{n}$ at time $t$, $dt\,\Omega \hat{f}_j(\vec{n}, \Omega)$ is the probability that a single $j$th reaction occurs in the next time interval $[t + dt)$ and $E_i^x$ is a step operator whose action on some function of $n_i$ is to change it to a function of $n_i + x$.[15] It has been shown using combinatorial arguments[15] that the microscopic rate function $\hat{f}_j(\vec{n}, \Omega)$ has the general form,

$$\hat{f}_j(\vec{n}, \Omega) = k_j \prod_{z=1}^{N} \Omega^{-s_{zj}} \frac{n_z!}{(n_z - s_{zj})!}. \tag{3}$$

By the Wiener-Khinchin theorem,[22] the one-sided power spectrum of the fluctuations in the number of molecules of species $i$ at stationary state is given by the Fourier transform of the autocorrelation of the number fluctuations in this species,

$$S_i(\omega) = \frac{1}{\pi} \int_{-\infty}^{\infty} e^{-i\omega\tau} \langle [n_i(t) - \langle n_i \rangle_{ss}][n_i(t + \tau) - \langle n_i \rangle_{ss}] \rangle d\tau, \tag{4}$$

where the angled brackets denote the statistical average, $t$ is any time for which steady-state conditions have been achieved and $\langle n_i \rangle_{ss}$ is the steady-state number of molecules of species $i$. A power spectrum peak at some frequency, $\omega = \hat{\omega}$ (the peak frequency), indicates the presence of oscillations in the number of molecules at this particular frequency.

The problem with the determination of the power spectrum lies in the fact that one cannot generally derive a closed form equation for the autocorrelation (and more generally for the moments) using the chemical master equation and hence an approximation method is needed.

### B. The linear-noise approximation

One means to circumvent this inherent analytical intractability involves expanding the master equation as a series in powers of the inverse square root of the compartment volume, a technique popularly referred to as the system-size expansion.[15]

To lowest order, i.e., in the limit of large volumes, it is found that the time-evolution equations for the mean concentrations predicted by the chemical master equation are the same as the conventional rate equations,

$$\frac{d}{dt}\vec{\phi} = \mathbf{S}\, \vec{f}(\vec{\phi}), \tag{5}$$

where $\vec{\phi} = \langle \vec{n} \rangle / \Omega$ is the mean concentration vector, $\mathbf{S}$ is the stoichiometric matrix with elements $S_{ij}$ and $\vec{f} = \lim_{\Omega \to \infty} \vec{\hat{f}}(\langle \vec{n} \rangle, \Omega)$. The fluctuations about the mean concentrations are given by a linear stochastic differential

equation,

$$d\vec{\xi}(t) = \mathbf{J}\vec{\xi}(t)\,dt + \mathbf{B}\,d\vec{W}(t), \tag{6}$$

where $\vec{\xi}(t) = \Omega^{1/2}(\frac{\vec{n}(t)}{\Omega} - \vec{\phi})$ and $d\vec{W}(t)$ is an $N$-dimensional Wiener process. The matrices $\mathbf{J}$ and $\mathbf{D} = \mathbf{B}\mathbf{B}^T$ are the Jacobian and diffusion matrices, respectively, which can be constructed directly from the rate equations and from the stoichiometric matrix; their elements are given by[23]

$$J_{ij} = \frac{\partial}{\partial \phi_j}\sum_{r=1}^{R} S_{ir} f_r, \tag{7}$$

$$D_{ij} = \sum_{r=1}^{R} S_{ir} S_{jr} f_r. \tag{8}$$

Equations (5) and (6) constitute the linear-noise approximation: a continuous stochastic approximation of the chemical master equation, Eq. (2), which is valid in the large volume limit.

The utility of this approximation lies in the fact that the linearity of Eq. (6) enables one to write down a closed form solution for the autocorrelation function, $\langle \xi_i(t)\xi_i(t+\tau)\rangle$ in terms of the elements of the Jacobian and diffusion matrices. The quantity $\Omega\langle \xi_i(t)\xi_i(t+\tau)\rangle$ is the linear-noise approximation estimate of the correlator $\langle [n_i(t) - \langle n_i\rangle_{ss}][n_i(t+\tau) - \langle n_i\rangle_{ss}]\rangle$ which appears in the spectrum definition, Eq. (4). The result is an approximate closed-form equation for the power spectrum of the number fluctuations[22]

$$S_i(\omega) = \frac{\Omega}{\pi}\left[[-\mathbf{J} + \mathbf{I}i\omega]^{-1}\mathbf{D}[(-\mathbf{J})^T - \mathbf{I}i\omega]^{-1}\right]_{ii}. \tag{9}$$

## III. A CLASSIFICATION OF NIO FOR TWO SPECIES SYSTEMS

In this section we restrict ourselves to chemical reaction schemes involving two species and use the linear-noise approximation result of Sec. II to explore the intimate relationship between the existence of NIO and the type of steady state (stable node or stable focus) in the deterministic equations.

For systems with only two interacting species, the resultant functional form of the spectrum equation, Eq. (9), for species $X_i$ is

$$S_i(\omega) = \frac{\Omega}{\pi}\frac{\alpha_i(\mathbf{J},\mathbf{D}) + \beta_i(\mathbf{D})\,\omega^2}{p(\mathbf{J}) + q(\mathbf{J})\,\omega^2 + \omega^4}, \tag{10}$$

where the parameteric dependencies on the Jacobian and diffusion matrices are explicitly shown. In particular, the functions $p$ and $q$ are equal to $\lambda_1^2\lambda_2^2$ and $\lambda_1^2 + \lambda_2^2$, respectively, where the $\lambda$'s are the eigenvalues of the Jacobian matrix, $\mathbf{J}$. For a stable node, the eigenvalues are real and negative while for a stable focus, the eigenvalues are a complex pair, $\lambda_{1,2} = -\mu \pm i\tilde{\omega}$ where both $\mu$ and $\tilde{\omega}$ are positive real numbers. Hence it follows that generally $p \in \mathbb{R}_{>0}$ and $q \in \mathbb{R}$. The parameter $\beta_i = D_{ii}$ and hence by Eq. (8) one can deduce that $\beta_i \in \mathbb{R}_{>0}$. Lastly, the parameter $\alpha_i$ has to be a positive real-valued number since $\alpha_i = (\pi/\Omega)pS_i(0)$.

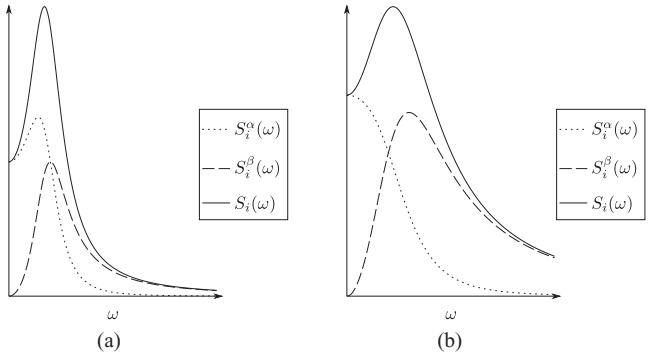


FIG. 1. Plots of the spectrum (11) along with the sub-spectra (12) showing the two possible ways in which a peak in the power spectrum can arise: (a) The parameters $p$ and $q$ are such that both sub-spectra have a peak ($p = 1$, $q = -1$) and a peak in $S_i(\omega)$ is guaranteed; (b) The parameters $p$ and $q$ are such that only the sub-spectrum $S_i^\beta$ has a peak ($p = 5$, $q = 1$), but the magnitude of $\beta_i$ is sufficiently large that a peak exists in $S_i(\omega)$.

We now decompose the spectrum Eq. (10) for a single species into two sub-spectra, $S_i^\alpha(\omega)$ and $S_i^\beta(\omega)$:

$$S_i(\omega) = \frac{\Omega}{\pi}\left(S_i^\alpha(\omega) + S_i^\beta(\omega)\right), \tag{11}$$

$$S_i^\alpha(\omega) = \frac{\alpha_i}{p + q\,\omega^2 + \omega^4}, \quad S_i^\beta(\omega) = \frac{\beta_i\,\omega^2}{p + q\,\omega^2 + \omega^4}. \tag{12}$$

It is easy to show that $S_i^\alpha(\omega)$ has a peak if $q < 0$ and that $S_i^\beta(\omega)$ always has a peak. Hence one can classify NIOs into two distinct cases (see Fig. 1 for an illustration):

- **Stability dominated NIO**: The parameter $q < 0$ and hence both sub-spectra have a peak, guaranteeing a peak in $S_i(\omega)$ (see Appendix A).
- **Noise dependent NIO**: The parameter $q \geq 0$ such that only the sub-spectrum $S_i^\beta$ has a peak, but the magnitude of $\beta_i$ relative to $\alpha_i$ is sufficiently large that a peak exists in $S_i(\omega)$. The exact criterion in this case is $\beta_i > \alpha_i q/p$ (see Appendix A).

The first case is termed stability dominated NIO because the existence of the NIO solely rests on the sign of $q$ which is a function of the eigenvalues of the Jacobian and hence of the type of steady state. The second case is termed noise dependent NIO because $\beta_i$ being a function of the diffusion matrix is a measure of the strength of the noise and this needs to be larger than a critical threshold for NIO to exist. Note the important implication that for the stability dominated NIO case, NIO present in one species dictates that NIO are present in the other species, however, this is not necessarily true for noise dependent NIO since the $\alpha_i$ and $\beta_i$ are species dependent.

Consider the case of stability dominated NIO. If we have a stable focus then the eigenvalues can be denoted as $\lambda_{1,2} = -\mu \pm i\tilde{\omega}$ where both $\mu$ and $\tilde{\omega}$ are positive real numbers. The condition $q < 0$ is then fulfilled if $\mu < \tilde{\omega}$, in other words if the time scale of decay of the amplitude of the damped oscillations in the deterministic model is larger than the period of the same oscillations.

Now we consider the case of noise dependent NIO. The condition $q \geq 0$ is satisfied for stable foci with $\mu \geq \tilde{\omega}$ and also for stable nodes, i.e., those steady states characterized by two real and negative eigenvalues. Hence these type of steady states can also be expected to give rise to NIO, this condition being dictated by the magnitude of the elements of the diffusion matrix.

Hence in summary it is clear that not only stable foci can give rise to NIO but that stable nodes can do as well. In the rest of this article we focus on studying the existence and properties of the latter type of NIO, which we refer to as stable node NIO.

## IV. GENERAL PROPERTIES OF STABLE NODE NIO

### A. Frequency of the oscillations

While one would expect that the frequency of stable foci NIO is close to the frequency of damped oscillations in the deterministic model, it is not at all clear what should be the frequency of stable node NIO. A simple expression for this can be deduced by differentiating $S_i(\omega)$ in Eq. (10), setting the resulting equation to zero and solving for the roots of the quartic in $\omega$. Using the fact that $q > 0$ for a node, one finds that the only positive (and hence admissible) solution for the peak frequency of NIO in species $i$ is

$$\hat{\omega}_i = \left( \frac{[p(p + q^2 x_i(x_i - 1))]^{1/2} - p}{q x_i} \right)^{1/2}, \qquad (13)$$

where $x_i = \beta_i p/\alpha_i q$. Note that the criterion for a peak for a noise dependent NIO (see Sec. III) implies $x_i > 1$. From the above equation we can see that $\hat{\omega}_i$ varies between 0 and a maximum value of $p^{1/4} = \sqrt{\lambda_1 \lambda_2}$. Hence the period of NIO in the node case is bounded from below by the geometric mean of the two decay time scales of non-oscillatory transients in the deterministic model.

Furthermore, one can deduce that the peak frequency increases monotonically with $x_i$ meaning that this frequency increases with the fraction of power contributed by the subspectrum $S_i^{\beta}(\omega)$ to the total power spectrum $S_i(\omega)$. It is also easy to show that the maximum peak frequency value of $p^{1/4}$ for $S_i(\omega)$ is equal to the peak frequency of the $S_i^{\beta}(\omega)$ subspectrum. These observations are intuitively clear since for a noise dependent NIO (of which a stable node NIO is a special case) only the $S_i^{\beta}(\omega)$ has a peak and hence its size relative to the peakless $S_i^{\alpha}(\omega)$ sub-spectrum crucially dictates the spectral properties of the NIO.

### B. Quality of the oscillations

Next we discuss the quality of the stable node NIO. A typical measure of oscillation quality is the Q-factor, defined as

$$Q = \frac{\hat{\omega}}{\Delta\omega}, \qquad (14)$$

where the bandwidth $\Delta\omega$ is the difference of the two frequencies at which the power takes its half-maximum value. To make connection with later developments, we denote this conventional $Q$-factor as $Q^{50\%}$.

The $Q^{50\%}$ of the spectrum $S_i(\omega)$ can be written as a function of two parameters, $R_\epsilon = \lambda_1/\lambda_2$ which is the ratio of the two real eigenvalues, and $R_{H\alpha\beta}$ which is the relative weighting of the $\alpha$ and $\beta$ subspectra, as quantified by the ratio of their maximum heights (see Fig. 2(a) for a contour plot). This choice of parameters is convenient because $R_\epsilon$ is a parameter which is dictated solely by deterministic stability considerations whereas $R_{H\alpha\beta}$ is a parameter which is determined by the properties of the internal noise. Note that $R_\epsilon$ is specified such

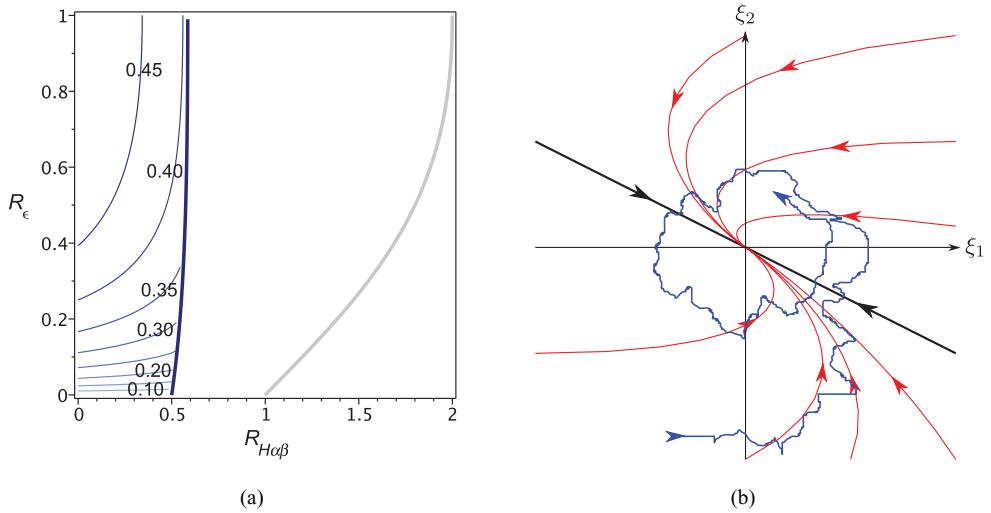


(a) (b)

FIG. 2. (a) The quality of stable node oscillations, as described by the conventional quality factor, $Q^{50\%}$. Contours of $Q^{50\%}$ (blue) are shown as a function of the two parameters $R_\epsilon$ and $R_{H\alpha\beta}$ (see text for definitions). The thick gray line demarks the parameter regions in which NIO are/are not observed and the thick dark blue line demarks the regions in which the peak is strong enough to obtain its half-maximum value on the low frequency side of the peak (i.e., $Q^{50\%}$ is defined). It is clear that $Q^{50\%}$ is not a suitable measure for describing the quality of weak stable node NIO as it is only defined for a small region of the full parameter space in which NIO is observed. (b) Illustration of an example noisy evolution of the fluctuation variables $\xi_1$, $\xi_2$ in a system with degenerate node stability, i.e., $R_\epsilon = 1$, corresponding to the maximum $Q^{50\%}$ case. Red curves are deterministic trajectories, the blue curve is the stochastic trajectory, and the black line is the single linearly independent eigenvector of the Jacobian.

that $|\lambda_1| < |\lambda_2|$. The quality of the NIO increases with increasing $R_\epsilon$ and with decreasing $R_{H\alpha\beta}$ and reaches a maximum of $Q^{50\%} = 1/2$ when $R_\epsilon = 1$ and $R_{H\alpha\beta} = 0$.

The first observation can be explained as follows. As $R_\epsilon$ approaches its maximum of one, it approaches the case of a stable degenerate node. Such a steady state lies at the node-focus borderline and is characterized in phase space by deterministic trajectories which approach the origin tangent to the single linearly independent eigenvector;[24] the deterministic trajectories in this case display a degree of curvature, in a sense trying to wind around in a spiral but not quite making it. The stochastic trajectories will follow to some extent the curvature of the deterministic trajectories and for some cases, the noise will cause the trajectory to close on itself hence leading to a noise-induced oscillation (see Fig. 2(b) for an illustration). Hence as one approaches the node-focus borderline, i.e., as $R_\epsilon \to 1$, one expects the quality of NIO to increase since the stochastic trajectories can sample increasingly curved deterministic trajectories. Note that similar arguments have been previously used to explain how the existence and properties of stable focus NIO are related to the curvature of the focus trajectories (see, for example, Ref. 25).

The observation that the quality increases with decreasing $R_{H\alpha\beta}$ is intuitively obvious when one considers that out of the two sub-spectra composing the total spectrum, only the $S_i^\beta(\omega)$ sub-spectrum has a peak, and hence its increased contribution to the total spectrum necessarily improves the quality. The same argument hints that that the maximum $Q^{50\%} = 1/2$ for the total spectrum $S_i(\omega)$ equals the $Q^{50\%}$ of the $S_i^\beta(\omega)$ sub-spectrum. This is indeed the case. The latter is given by the remarkably simple expression,

$$Q^{50\%}_{S^\beta} = \frac{\sqrt{R_\epsilon}}{(R_\epsilon + 1)}, \tag{15}$$

which maximizes at a value of 1/2 when the eigenvalues become equal.

In Fig. 2(a), it is observed that there is a large region of parameter space for which NIO exist (this is the area between the thick blue and gray lines in the figure), but the shape of the power spectrum is such that it does not fall to its half-maximum value on the low frequency side of the peak and hence a $Q^{50\%}$ cannot be defined. To allow a measure of quality over a greater range of the parameter space, we introduce a more general version of the conventional $Q$-factor in Eq. (14): $Q^{f\%} = \hat{\omega}/\Delta\omega^{f\%}$, where $f \in (0, 100)$ and $\Delta\omega^{f\%}$ is the difference of the frequencies at which the spectrum takes $f$ % of its maximum value. We choose to use the $Q$-factor $Q^{99\%}$ in order to describe the vast majority of the region which cannot be captured by the $Q^{50\%}$ measure.

This measure, while more complicated analytically than $Q^{50\%}$, is also a function of only $R_\epsilon$ for $S_i^\beta(\omega)$ and a function of $R_\epsilon$ and $R_{H\alpha\beta}$ for $S_i(\omega)$, and shows very similar behaviour to the $Q^{50\%}$ measure over the parameter regions in which $Q^{50\%}$ is defined (compare the blue contours in Figs. 2(a) and 3). It can be shown that the maximum possible value of $Q^{99\%}$ is $3\sqrt{11}/2 \simeq 5$. The $Q^{99\%}$ measure only uses spectrum information very close to the peak frequency; it is a very localized measure which directly captures the high curvature at the peak. However, we note that the measure successfully

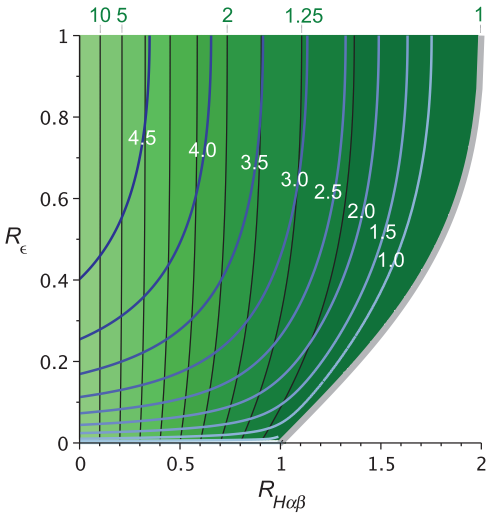


FIG. 3. The quality of stable node oscillations, as described by $Q^{99\%}$. Contours of $Q^{99\%}$ (blue) are shown as a function of the two parameters $R_\epsilon$ and $R_{H\alpha\beta}$. Green filled contours show the variation of the amplification factor $\frac{S_i(\hat{\omega})}{S_i(0)}$, with selected contour values shown. The thick gray line demarks the parameter regions in which NIO are/are not observed.

captures the behaviour of the spectrum over wider frequency ranges. As an example, a large amplification value $\frac{S_i(\hat{\omega})}{S_i(0)}$ (ratio of the power at the peak frequency to the power at zero frequency) has been highlighted as being an important parameter in describing pronounced stochastic oscillations.[16] In Fig. 3 this amplification factor is also shown (lighter green contours represent higher amplification), and it is observed that it is not possible to obtain a very high $Q^{99\%}$ value without an associated high amplification value. Further validation of the $Q^{99\%}$ factor as a reliable measure of stable node quality can be found in Appendix B.

We note that it is difficult to further develop the general theory of stable node NIO for biochemical systems with internal noise because generally the **J** and **D** matrices are both dependent on the rate constants in the system as well as the steady-state values of concentrations of the rate equations (see Eqs. (7) and (8)). This places important constraints on the values that can be taken by the parameters $\alpha_i(\mathbf{J}, \mathbf{D})$ and $\beta_i(\mathbf{D})$ and hence constraints on the region of parameter space where stable node NIO exist. Hence the rest of this article is devoted to understanding stable node NIO in the context of specific biochemical systems.

## V. TWO SPECIES BIOCHEMICAL SYSTEMS WITH STABLE NODE NIO

In this section we use the linear-noise approximation to study the relationship between the type of steady state and the existence of NIO for three biochemical systems involving the interaction of two species. These numerical classifications are listed in Table I. For selected points in parameter space where stable node NIO are predicted to exist, we use the periodogram method to numerically estimate the power spectra from stochastic simulations using the stochastic simulation algorithm (see Appendix C) and compare these with the theoretical spectra predicted by the linear-noise approximation. In

TABLE I. Existence of NIO and linear stability classifications as used in Figures 4, 7, and 11.

| | Classification | |
|---|---|---|
| Numerical ID | NIO | Stability of steady state |
| 0 | None | Unstable |
| 1 | Species $A$ | Node |
| 2 | Species $A$ | Focus |
| 3 | Species $B$ | Node |
| 4 | Species $B$ | Focus |
| 5 | $A$ and $B$ | Node |
| 6 | $A$ and $B$ | Focus |
| 7 | None | Node |
| 8 | None | Focus |

all cases we find good agreement with the two spectra, and hence verify that a peak in the power spectrum of number fluctuations does indeed exist for certain stable node steady states. We shall also investigate the relationship between the $Q^{99\%}$ quality factor of stable NIO and the distance of the node from the node-focus borderline in phase space, as well as the robustness of the linear-noise approximation predictions for small molecule numbers.

### A. Example 1: The Brusselator

The Brusselator is the only known chemical scheme involving just two interacting species and whose deterministic equations admit limit cycle oscillations,[26–29]

$$\oslash \xrightarrow{k_0} A, \quad 2A + B \xrightarrow{k_1} 3A, \quad A \xrightarrow{k_2} B, \quad A \xrightarrow{k_3} \oslash. \tag{16}$$

The autocatalytic step $2A + B \to 3A$ is not an elementary reaction but rather an effective reaction composed of simpler reaction steps (more on this later). The possible biological relevance of this reaction scheme stems from the fact that the autocatalytic step can be produced by a series of enzyme-catalyzed reactions.[28]

We start by defining two dimensionless parameters

$$\Lambda_1 = \frac{k_0^2 k_1}{k_3^3}, \quad \Lambda_2 = \frac{k_2}{k_3}. \tag{17}$$

The stoichiometric matrix and the macroscopic rate function vector for this system are

$$\mathbf{S} = \begin{pmatrix} 1 & 1 & -1 & -1 \\ 0 & -1 & 1 & 0 \end{pmatrix}, \tag{18}$$

$$\vec{f} = \{k_0, k_1[A]^2[B], k_2[A], k_3[A]\}^T, \tag{19}$$

where $[A]$ and $[B]$ are the macroscopic concentrations of species $A$ and $B$. The rate equations are then given by $\{\partial_t[A], \partial_t[B]\}^T = \mathbf{S}\vec{f}$. Linear stability analysis of these equations reveals that the regions in $\Lambda_1$-$\Lambda_2$ space which characterize a stable node and a stable focus respectively are

$$\Lambda_1 > \Lambda_2 - 1, \quad 1 + (\Lambda_1 - \Lambda_2)^2 - 2(\Lambda_1 + \Lambda_2) \geq 0, \tag{20}$$

$$\Lambda_1 > \Lambda_2 - 1, \quad 1 + (\Lambda_1 - \Lambda_2)^2 - 2(\Lambda_1 + \Lambda_2) < 0. \tag{21}$$

Now we use the linear-noise approximation to deduce the conditions for the existence of NIO. Substituting the stoichiometric matrix and rate function vector into Eqs. (7) and (8) we obtain the Jacobian and diffusion matrices. Finally substituting the latter in Eq. (9) we obtain equations for $S_1(\omega)$, the power spectrum of species $A$, and for $S_2(\omega)$, the power spectrum of species $B$. The latter equations are of the form given by Eq. (10) with global parameters $p = k_3^4\Lambda_1^2$, $q = k_3^2(1 + (\Lambda_1 - \Lambda_2)^2 - 2\Lambda_2)$ and species-specific parameters given by

$$\alpha_1 = 2k_0k_3^2\Lambda_1^2, \tag{22}$$

$$\beta_1 = 2k_0(1 + \Lambda_2), \tag{23}$$

$$\alpha_2 = 2k_0k_3^2\Lambda_2(1 + \Lambda_2), \tag{24}$$

$$\beta_2 = 2k_0\Lambda_2. \tag{25}$$

Differentiating the expressions for $S_1(\omega)$ and $S_2(\omega)$ with respect to $\omega$, one finds the conditions for the peak in the power spectrum and hence for the existence of NIO in the number fluctuations of species $A$ and of species $B$, respectively, are

$$(\Lambda_1 - \Lambda_2)^2 - 3\Lambda_2 < 0, \tag{26}$$

$$\Lambda_2(1 + 2\Lambda_1 + \Lambda_2 - (\Lambda_1 - \Lambda_2)^2) - 1 > 0. \tag{27}$$

In Fig. 4(a) we plot in $\Lambda_1$-$\Lambda_2$ space the inequalities Eqs. (20) and (21) which determine the type of steady state (solid black line), together with the inequalities Eqs. (26) and (27) which determine the existence of NIO (red and blue lines). The intersection of the regions defined by these inequalities are numbered according to the classification set forth in Table I. A large region of the space, i.e., region 6, exhibits NIO in both species and the steady state is a focus. This is the conventionally studied case. However, one can also see that there is a region, namely region 1, wherein the steady state is a node but there are NIO for species $A$. Interestingly there is no region where there are NIO in species B and the steady state is a node. We shall return to this point in Sec. VII.

In Fig. 4(b) we plot the $Q^{99\%}$ quality factor for region 1 in Fig. 4(a). This shows that, broadly speaking, the quality of the stable node NIO increases with decreasing distance from the node-focus boundary. This relationship is only approximate, however, the reason being that the quality is also significantly influenced by the properties of internal noise which are not single handedly captured by the Jacobian of the rate equations. In Fig. 5 we show the spectra obtained from the linear-noise approximation and from stochastic simulations for the three points marked by white circles in Fig. 4(b). A comparison of cases (a) and (b) in this figure shows the large difference in quality factor even though the location of the nodes in $\Lambda_1$-$\Lambda_2$ space puts both of them approximately the same distance from the node-focus border (see Fig. 4(b)). In all cases we find good agreement between theory and simulations confirming the existence of stable node NIO.

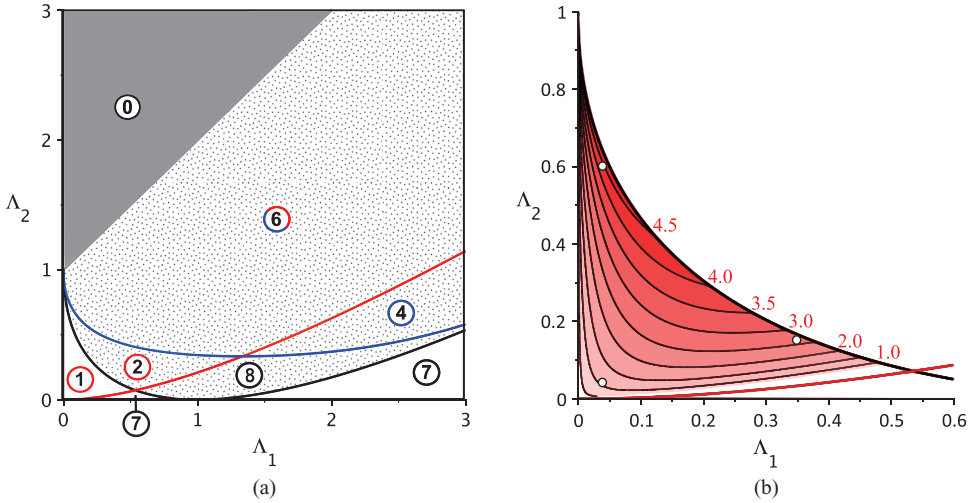


FIG. 4. (a) NIO existence and stability classification for the Brusselator in $\Lambda_1$-$\Lambda_2$ space. Number classifications are as in Table I. Red (blue) circles are used to emphasize the existence of NIO in the number fluctuations of species $A$ ($B$); the dotted region corresponds to the stable focus regime; white regions correspond to the stable node regimes and the gray region is where the fixed point is unstable (limit cycle). (b) Contour plot of the variation of the Q factor $Q^{99\%}$ with $\Lambda_1$, $\Lambda_2$ in the stable node regime (① in (a)). The black contour lines, labelled with red numbers, represent $Q^{99\%}$ values from 0.5 to 4.5 in 0.5 increments. White circles indicated on the $Q^{99\%}$ ($\Lambda_1$, $\Lambda_2$) surface correspond to the three power spectra in Figure 5.

### 1. Finite volume effects and elementary reaction versions of the Brusselator

We used stochastic simulations to explore two further questions: (i) given that the linear-noise approximation theory is valid in the limit of large volumes/large molecule numbers, how well do its results for stable node NIO hold when one has small volume/small molecule numbers? (ii) the Brusselator is composed of one trimolecular reaction, a reaction which in practice occurs very rarely due to the unlikely event of three colliding molecules[30] (though important in atom and diatom recombination and collision-induced reactions[30–32]). Thus in many instances such a reaction approximately models a set of underlying (fast) elementary (unimolecular and bimolecular) reactions. Is it the case that stable node NIO can also be predicted from elementary reaction models of the Brusselator?

The first question is important since molecule numbers of many species inside cells are quite small, typically in the range of few tens to few thousands.[8,9] In Fig. 6 we show the results of stochastic simulations investigating how the power spectra for the parameter sets ($a$) and ($b$) used in Fig. 5 change with decreasing volume and a corresponding decrease in the mean molecule numbers of species $A$. The linear-noise approximation result is shown as a solid line. Note that in both cases the linear-noise theory is accurate for mean molecule numbers of the order of a thousand molecules. For parameter set (b) the theory remains remarkably accurate for mean molecule numbers less than that of a single molecule while for parameter set (a) considerable deviations from the theory are evident for mean molecule numbers below a hundred molecules. In particular one observes a clear deterioration of quality with decreasing mean molecule numbers. These results show that stable node NIO can exist for molecule numbers typical of those inside cells and suggest that the quality of the spectra predicted by the linear-noise approximation provides an upper bound for the quality of spectra at finite mean molecule numbers (finite volumes).

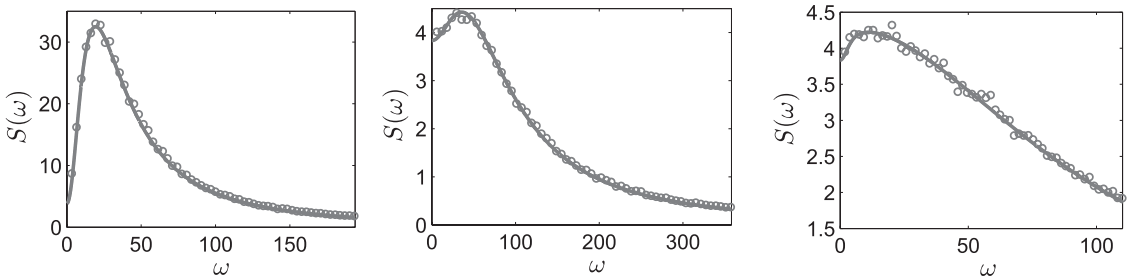


FIG. 5. Power spectrum plots of the number fluctuations in species $A$ in the Brusselator reaction system for three different sets of dimensionless parameters for which a stable node steady state exists. Solid lines show the analytical spectrum from the linear-noise approximation; open circles show the numerical spectrum calculated by averaging the periodograms of 2500 realizations of the stochastic simulation algorithm. The constants are $\Omega = 1 \times 10^{-15} l$, $k_0 = 1 \times 10^{-4}$ M s$^{-1}$, and $k_3 = 100$ s$^{-1}$. In addition $k_1$ and $k_2$ take values of $4 \times 10^{12}$ M$^{-2}$ s$^{-1}$ and 60 s$^{-1}$ for case (a), $3.5 \times 10^{13}$ M$^{-2}$ s$^{-1}$ and 15 s$^{-1}$ for case (b) and $4 \times 10^{12}$ M$^{-2}$ s$^{-1}$ and 4 s$^{-1}$ for case (c). Note that the units for concentration, time and frequency $\omega$ are Molar (M), second (s), and radians per second (rad s$^{-1}$), respectively.

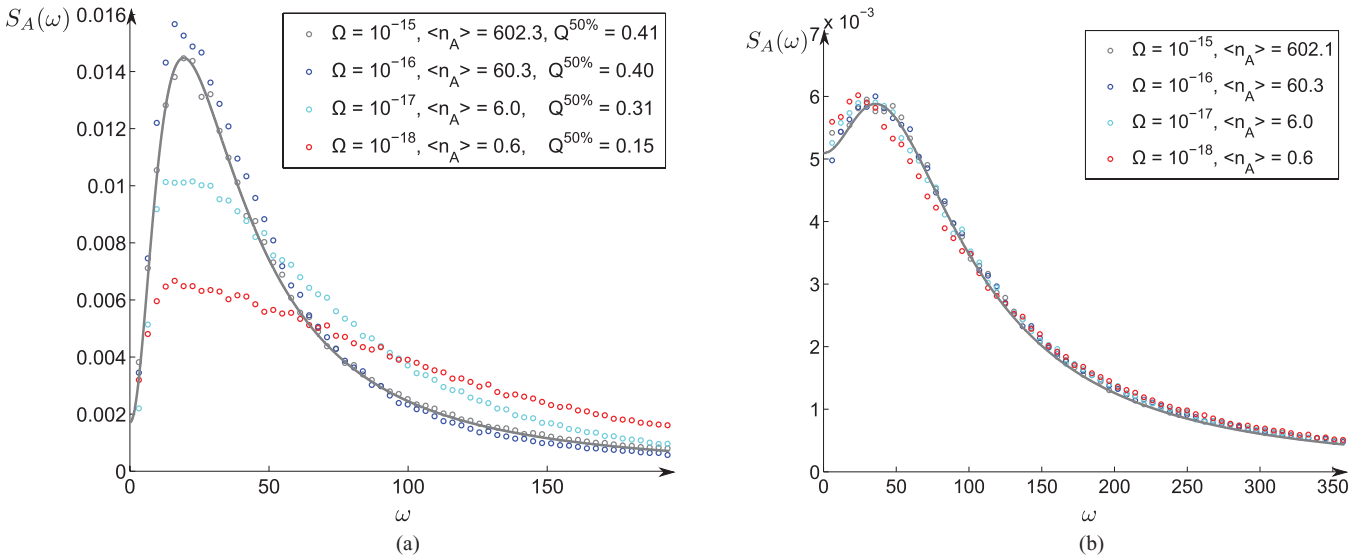


FIG. 6. Normalized power spectrum plots of the number fluctuations in species $A$ in the Brusselator reaction system for parameter sets (a) and (b) in Fig. 5, as a function of compartment volume Ω. Solid lines show the analytical spectrum (normalized by the total power) from the linear-noise approximation; open circles show the normalized numerical spectrum for each reaction volume, calculated by averaging the periodograms of 2500 realizations of the stochastic simulation algorithm and then normalizing by the total power (sum of all spectrum values × frequency resolution). In the figure legends, compartment volumes Ω are shown in units of litres, $\langle n_A \rangle$ is the steady-state mean number of molecules of $A$ and $Q^{50\%}$ is the quality factor calculated from the numerical power spectrum (see Appendix D for details). The unit for frequency $\omega$ is rad s$^{-1}$.

The importance of the second question stems from the fact that the linear-noise approximation can generally give different results for effective models and their elementary versions[33,34] and hence there exists the possibility that the stable node NIO is an artifact of modeling a trimolecular reaction. We simulated an elementary reaction version of the Brusselator put forward by Cook *et al.*[35] where the trimolecular reaction $2A + B \to 3A$ is broken down into the pair of bimolecular reactions: $A + A \rightleftharpoons X$, $X + B \to X + A$ (this is labeled Scheme III in the aforementioned article). The system displayed stable node NIO with similar quality (data not shown) which hence verifies that such oscillations are not an artifact of the non-elementary reaction in the Brusselator. Further support to this conjecture will be evident in the next subsections where we study two systems composed of purely elementary reactions and in both cases we find stable node NIO.

### B. Example 2: A simpler autocatalytic reaction

We now consider another autocatalytic reaction scheme in which two distinct species are input to a reaction volume wherein they are involved in a bimolecular autocatalytic reaction, before the product species is exported from the reaction volume,

$$\oslash \xrightarrow{k_0} A, \quad \oslash \xrightarrow{k_1} B, \quad A + B \xrightarrow{k_2} 2B, \quad B \xrightarrow{k_3} \oslash. \tag{28}$$

This reaction is simpler than the Brusselator and indeed more realistic in the sense that it is composed of at most bimolecular (and hence elementary) reactions. It is also the case that such autocatalytic reactions appear in various biological contexts such as the autocatalytic conversion of normal prion protein to its pathogenic form,[36] and the activation of MPF (maturation promoting factor) complex in the cell division cycle.[37]

Its analysis proceeds as for the previous example. We define two non-dimensional parameters,

$$\Lambda_1 = \frac{k_1}{k_0}, \quad \Lambda_2 = \frac{k_0 k_2}{k_3^2}. \tag{29}$$

The stoichiometric matrix and the macroscopic rate function vector for this system are

$$\mathbf{S} = \begin{pmatrix} 1 & 0 & -1 & 0 \\ 0 & 1 & 1 & -1 \end{pmatrix}, \tag{30}$$

$$\vec{f} = \{k_0, k_1, k_2[A][B], k_3[B]\}^T, \tag{31}$$

from which we obtain the deterministic rate equations $\{\partial_t[A], \partial_t[B]\}^T = \mathbf{S}\vec{f}$. Note that in contrast with the Brusselator, this system's deterministic rate equations do not exhibit limit cycle behaviour. Linear stability analysis of the rate equations shows that its steady state is a node if the condition

$$(\Lambda_1 + (1 + \Lambda_1)^2\Lambda_2)^2 - 4(1 + \Lambda_1)^3\Lambda_2 \geq 0, \tag{32}$$

is satisfied; otherwise the steady state is a focus. The linear-noise analysis proceeds as before, namely one uses Eqs. (7) and (8) to construct the Jacobian and diffusion matrices from $\mathbf{S}$ and $\vec{f}$ and then substitutes these into Eq. (9) to obtain the spectra equations: $S_1(\omega)$ for species $A$, and $S_2(\omega)$, for species $B$. The latter equations are of the form given by Eq. (10) with global parameters $p = k_3^4(1 + \Lambda_1)^2\Lambda_2^2$, $q = k_3^2(\Lambda_1^2 - 2(1 + \Lambda_1)^2\Lambda_2 + (1 + \Lambda_1)^4\Lambda_2^2)/(1 + \Lambda_1)^2$ and species-specific parameters given by

$$\alpha_1 = 2k_0k_3^2, \tag{33}$$

$$\beta_1 = 2k_0, \tag{34}$$

$$\alpha_2 = 2k_0k_3^2\Lambda_2^2(1 + \Lambda_1)^3, \tag{35}$$

$$\beta_2 = 2k_0(1 + \Lambda_1). \tag{36}$$

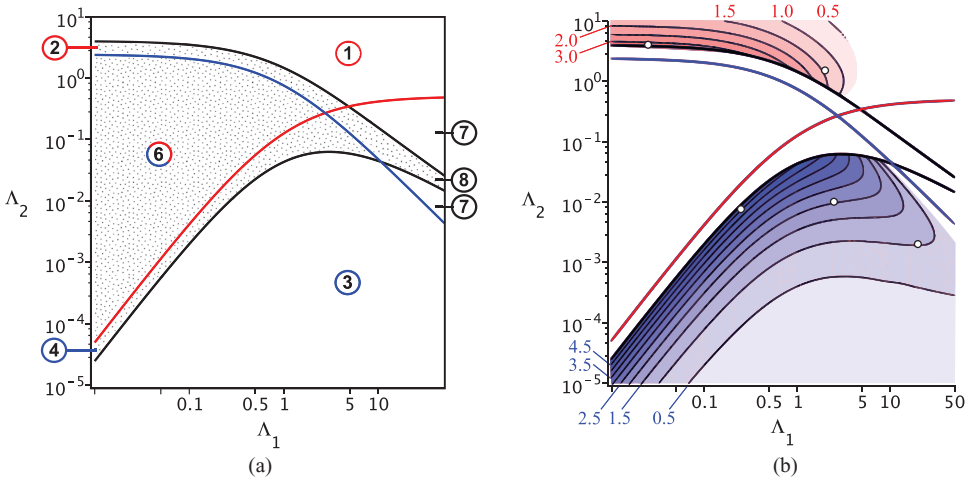


FIG. 7. (a) NIO existence and stability classification for a simple autocatalytic reaction system in $\Lambda_1$-$\Lambda_2$ space. Number classifications are as in Table I. Red (blue) circles are used to emphasize the existence of a peak in the power spectrum of species $A$ ($B$); the dotted region corresponds to the stable focus regime; white regions correspond to the stable node regimes. (b) Contour plot of the variation of the Q factor $Q^{99\%}$ with $\Lambda_1$, $\Lambda_2$ in the stable node regimes (① and ③ in (a)). The black contour lines, labelled with red (for species $A$) and blue numbers (for species $B$), represent $Q^{99\%}$ from 0.5 to 4.5 in 0.5 increments. Open circles indicated on the $Q^{99\%}$ ($\Lambda_1$, $\Lambda_2$) surface correspond to the $\Lambda$ values of the five power spectra in Figs. 8 and 9.

Maxima of the power spectra at non-zero frequencies (and hence NIO) for species $A$ and $B$, respectively, occur when the conditions:

$$2(1+\Lambda_1)^2\Lambda_2 - \Lambda_1^2 > 0, \tag{37}$$

$$1 + 2\Lambda_1 + (1+\Lambda_1)^2\Lambda_2(2-(1+\Lambda_1)^2\Lambda_2) > 0, \tag{38}$$

are satisfied. From the inequalities Eqs. (32), (37), and (38) we obtain the complete phase space plot of the system's deterministic and NIO behaviour (see Fig. 7(a)). Note that unlike for the Brusselator, stable node NIO are possible for both species, i.e., regions 1 and 3. However note that it is not possible to have simultaneously stable node NIO in both species; this situation is only achievable for stable focus NIO (region 6, Figure 7(a)). In Fig. 7(b) we show the $Q^{99\%}$ quality measure of stable node NIO in both species (hues of red indicate the strength of NIO in $A$ and hues of blue indicate the strength of NIO in $B$). Note that as for the case of the Brusselator, there is a degree of correlation between the quality and the distance from the node-focus borderline in phase space; it is also found that the quality of NIO in species $B$ are better than those in species $A$.

We again present the power spectra from the linear-noise approximation alongside simulation results for the simple autocatalytic system for selected parameter sets (see Figs. 8 and 9). The locations of these parameter sets in phase space are shown as white circles in Fig. 7(b). In all cases the linear-noise approximation and simulation results agree very well, confirming the existence of stable node NIO in a chemical system with no limit cycle behaviour. It is also noteworthy that the $Q^{99\%}$ measure corresponds well with the more visually pronounced, sharp peaks in the power spectra which indicates its general usefulness in quantifying the quality of NIO of all types.

As mentioned in Sec. IV, the maximum $Q^{99\%}$ of a stable node which can be observed in a two species system is ≈5. The simple autocatalytic reaction can give rise to NIO with quality approaching this maximum (see Fig. 9(a)). However, stochastic trajectories of these near-maximum quality NIO, as produced by the stochastic simulation algorithm, give rise to oscillations in the time series data which are generally not easily discernible by the naked eye. An example of the most visually observable NIO that can be expected using the parameters for the high and low $Q$ cases of Figs. 9(a) and 9(c) are presented in Fig. 10. An approximation of the visually observable underlying oscillation is represented by a running time average of the data (dotted line). As well as aiding the reader in visualising the shape and regularity of the NIO, we note that this running time average provides a simple measure of the proportion of the variance in the data which is attributable to the visually discernible oscillatory behaviour. For the high $Q$ and low $Q$ parameters, the oscillation obtained from time averaging accounts for 54% and 22% of the variance of the non-time averaged data respectively. This again supports the quality measure used to describe the weak NIO in this article.

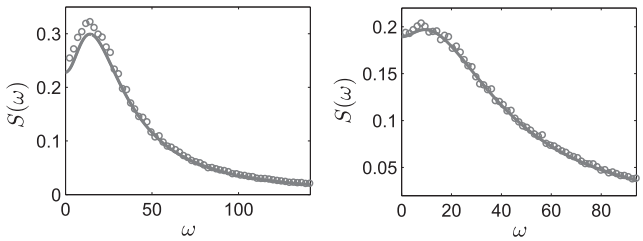


(a) $\Lambda_1 = 2.5 \times 10^{-2}, \Lambda_2 = 4$: $Q^{99\%} = 3.21$ (b) $\Lambda_1 = 2, \Lambda_2 = 1.5$: $Q^{99\%} = 1.43$

FIG. 8. Power spectrum plots of number fluctuations in species $A$ in the autocatalysis reaction system for two different sets of dimensionless parameters for which a stable node steady state exists. Solid lines show the analytical spectrum from the linear-noise approximation; open circles show the numerical spectrum calculated by averaging the periodograms of 5000 realizations of the stochastic simulation algorithm. The parameters common to both cases are: $\Omega = 1 \times 10^{-15} l$, $k_0 = 1 \times 10^{-6}$ M s$^{-1}$, $k_3 = 10$ s$^{-1}$. The case specific rate constants are: (a) $k_1 = 2.5 \times 10^{-8}$ M s$^{-1}$, $k_2 = 4 \times 10^{8}$ M$^{-1}$ s$^{-1}$ and (b) $k_1 = 2 \times 10^{-6}$ M s$^{-1}$, $k_2 = 1.5 \times 10^{8}$ M$^{-1}$ s$^{-1}$. The unit for frequency $\omega$ is rad s$^{-1}$.

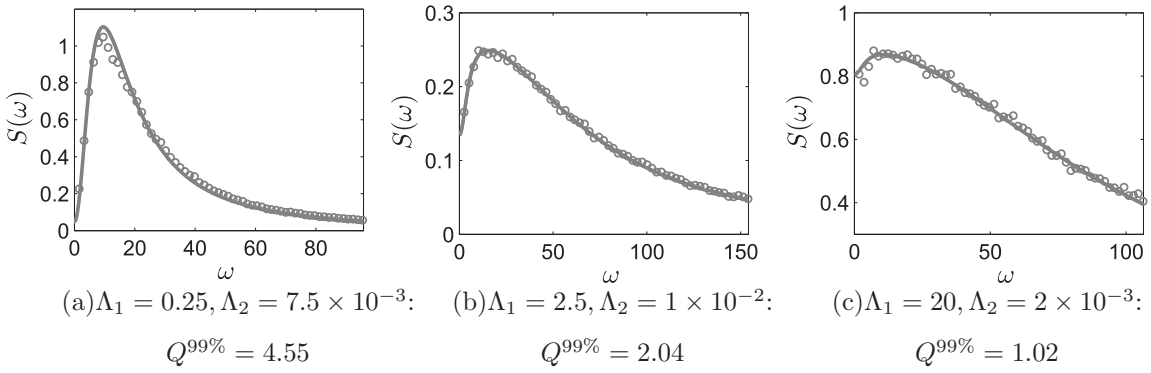


FIG. 9. Power spectrum plots of number fluctuations in species $B$ in the autocatalysis reaction system for three different sets of dimensionless parameters for which a stable node steady state exists. Solid lines show the analytical spectrum from the linear-noise approximation; open circles show the numerical spectrum calculated by averaging the periodograms of 5000 realizations of the stochastic simulation algorithm. The parameters common to both cases are: $\Omega = 1 \times 10^{-15} l$, $k_0 = 1 \times 10^{-6}\,\mathrm{M\,s^{-1}}$, $k_3 = 100\,\mathrm{s^{-1}}$. The case specific rate constants are: (a) $k_1 = 2.5 \times 10^{-7}\,\mathrm{M\,s^{-1}}$, $k_2 = 7.5 \times 10^{7}\,\mathrm{M^{-1}\,s^{-1}}$; (b) $k_1 = 2.5 \times 10^{-6}\,\mathrm{M\,s^{-1}}$, $k_2 = 1 \times 10^{8}\,\mathrm{M^{-1}\,s^{-1}}$; (c) $k_1 = 2 \times 10^{-5}\,\mathrm{M\,s^{-1}}$, $k_2 = 2 \times 10^{7}\,\mathrm{M^{-1}\,s^{-1}}$. The unit for frequency $\omega$ is $\mathrm{rad\,s^{-1}}$.

### C. Example 3: Trimerization reaction

We now study a simple reaction scheme which describes a trimerization process,

$$\oslash \xrightarrow{k_0} A, \quad 2A \xrightarrow{k_1} B, \quad A + B \xrightarrow{k_2} \oslash. \tag{39}$$

In this scheme the monomer $A$ is produced, binds to another $A$ to form the dimer $B$, and finally both monomer and dimer bind to form a trimer. The trimer is not explicitly represented in this two-species model. Independent of whether it accumulates, decays, or simply exits from the reaction volume, no effect is observed on the behaviour of $A$ or $B$ since the last reaction step is irreversible. This simple reaction is of relevance to various biological situations such as the trimerization of receptor proteins and of heat-shock factors.[38,39]

As we shall see the behaviour of this system can be quantified by means of a single non-dimensional parameter

$$\Lambda = \frac{k_1}{k_2}. \tag{40}$$

As before from the stoichiometric and macroscopic rate function vector one obtains both the type of steady state and the linear-noise approximation. We here just state the relevant results. The condition for a stable node is

$$1 + \Lambda(25\Lambda - 14) \geq 0. \tag{41}$$

A stable focus is obtained otherwise; similar to the simple autocatalysis scheme previously studied, there is no Hopf bifurcation in the system and hence no deterministic oscillations are possible. The linear-noise analysis gives power spectra of the form given by Eq. (10) with global parameters $p = 4k_0^2 k_2^2$, $q = k_0 k_2 (1 + \Lambda(25\Lambda - 2))/3\Lambda$ and species-specific parameters given by

$$\alpha_1 = 4k_0^2 k_2 / 3\Lambda, \tag{42}$$

$$\beta_1 = 8k_0/3, \tag{43}$$

$$\alpha_2 = 16 k_0^2 k_2 \Lambda / 3, \tag{44}$$

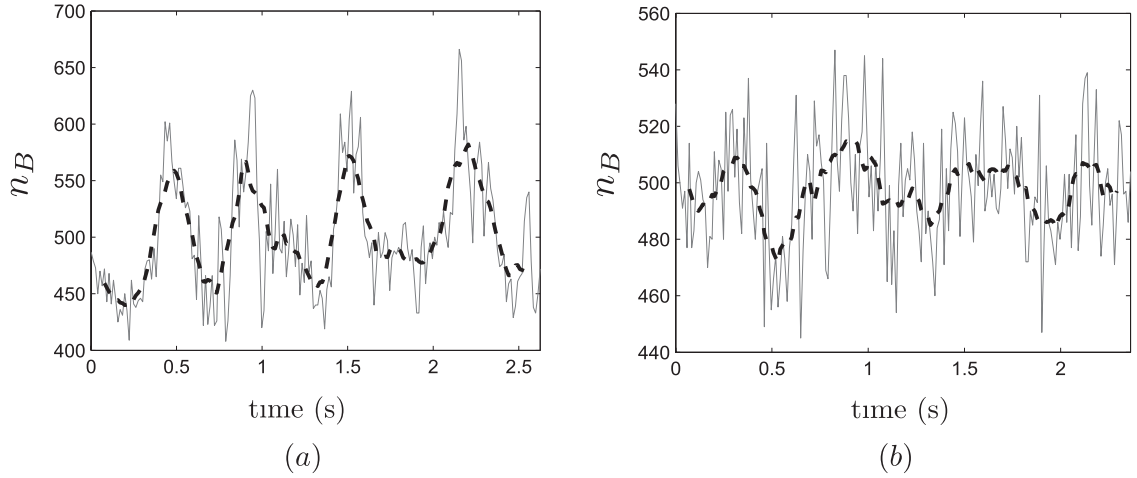


FIG. 10. Time series plots of the number of $B$ molecules in the autocatalysis reaction system for (a) the kinetic parameters of the high $Q$ case in Fig. 9(a); (b) the kinetic parameters of the low $Q$ case in Fig. 9(c). For each case 100 realizations of the stochastic simulation algorithm were obtained and the time series with the most visually observable oscillation is here shown. To allow fair comparison, volumes were chosen in each case to give a mean number of $B$ molecules $\langle n_B \rangle = 500$. Based on the characteristic period $T$ found from the peak frequencies of the linear noise approximation spectra in Figs. 9(a) and 9(c), four period-lengths of data were recorded at time intervals $\Delta t = \frac{1}{50} T$. In each figure, the solid line is the simulated data and the dotted line is a running average of the data over 13 points (approximately one quarter of a period).

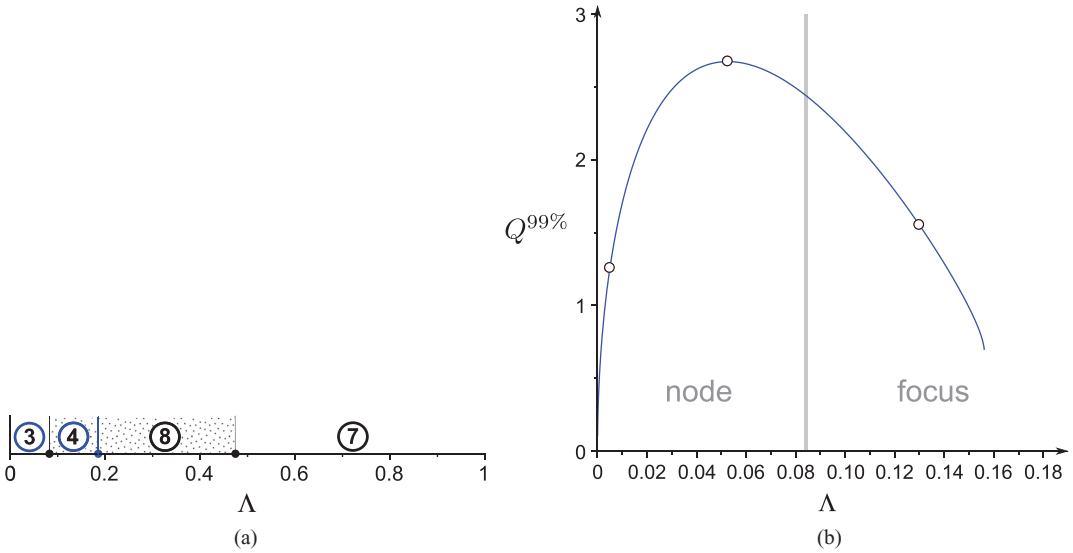


FIG. 11. (a) NIO existence and stability classification for the trimerization system with the parameter Λ. Number classifications are as in Table I. Blue circles are used to emphasise the existence of a peak in the power spectrum of variable $B$; the dotted region corresponds to the stable focus regime whereas white regions correspond to the stable node regimes. (b) Variation of the Q factor $Q^{99\%}$ with Λ (regions ③ and ④ in (a)). Open circles indicated on the $Q^{99\%}$ (Λ) curve correspond to the Λ values of the three power spectra in Fig. 12.

$$\beta_2 = 2k_0/3. \tag{45}$$

From these we deduce that the conditions for the existence of NIO in species $A$ and $B$ are

$$(\Lambda - 1)^2 < 0, \tag{46}$$

$$1 + 4\Lambda - 50\Lambda^2 > 0. \tag{47}$$

Note that the first of these two conditions cannot be met and hence there are no NIO in species $A$; however NIO is possible for species $B$. Plotting the inequalities Eqs. (41) and (47) we obtain the phase space diagram for the existence of species $B$ NIO in stable node and focus regions (see Fig. 11(a)). The theoretical quality factor of the stable node and stable focus NIO (regions 3 and 4) are shown in Fig. 11(b). The maximum quality of this extremely simple system is limited ($Q^{99\%} = 2.67$) in comparison to the simple autocatalysis and Brusselator schemes. A comparison of linear-noise approximation and simulation derived power spectra at three Λ values (whose position in phase space is marked by open circles in Fig. 11(b)) are shown in Fig. 12; the spectra are in good agreement and as for previous cases confirm the existence of stable node NIO. The simulations also confirm that optimal quality is obtained in the stable node regime, and not in the stable focus regime. This is intriguing given that one would expect noise to generate the largest oscillations by exciting the resonant frequencies of the damped oscillations in the focus regime; furthermore this clearly shows that the quality is not always inversely proportional to the distance from the node-focus borderline.

## VI. STABLE NODE NIO IN CASCADE CHEMICAL REACTION SYSTEMS

As mentioned in Sec. II, the maximum $Q^{99\%}$ of a stable node which can be observed in a two species system is ≈5. In Sec. III, we saw how both the Brusselator and the simpler autocatalytic reaction can give rise to NIO with quality approaching this maximum (see Figs. 5(a) and 9(a)). However

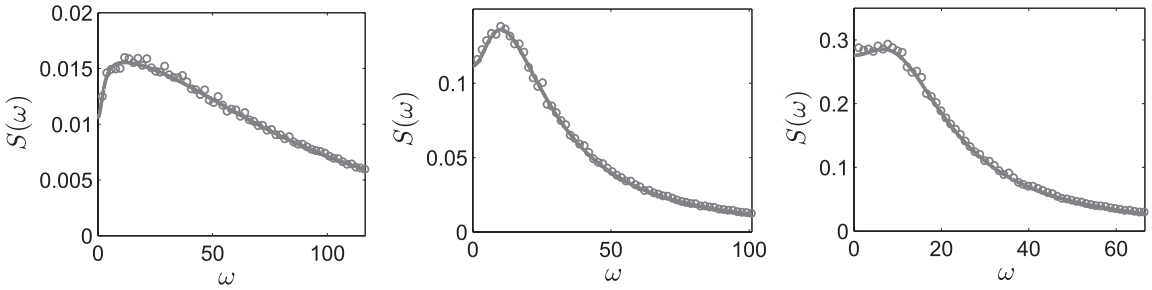


FIG. 12. Power spectrum plots of number fluctuations in species $B$ in the trimerization reaction system for three different sets of dimensionless parameters for which a stable node steady state exists. Solid lines show the analytical spectrum from the linear-noise approximation; open circles show the numerical spectrum calculated by averaging the periodograms of 2500 realizations of the stochastic simulation algorithm. The parameters common to both cases are: $\Omega = 1 \times 10^{-15} l$, $k_0 = 1 \times 10^{-6}$ M s$^{-1}$, $k_2 = 1.204 \times 10^8$ M$^{-1}$ s$^{-1}$. The case specific rate constant is: (a) $k_1 = 6.022 \times 10^5$ M$^{-1}$ s$^{-1}$; (b) $k_1 = 6.339 \times 10^6$ M$^{-1}$ s$^{-1}$; (c) $k_1 = 1.566 \times 10^7$ M$^{-1}$ s$^{-1}$. The unit for frequency $\omega$ is rad s$^{-1}$.

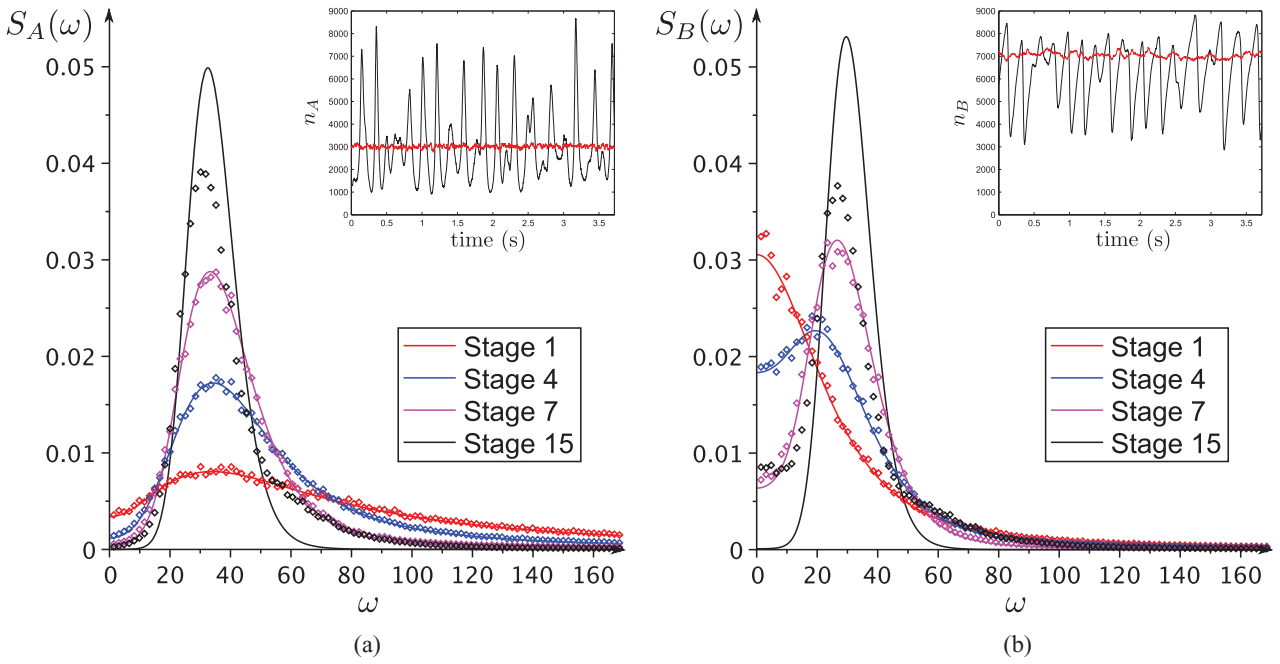


FIG. 13. Normalized power spectrum plots of the number fluctuations in species $A$ (a) and in species $B$ (b) involved in the cascade Brusselator reaction system illustrated in scheme (48) with $N = 15$. The parameters are $\Lambda_1 = 0.15$ and $\Lambda_2 = 0.35$, as defined in Eq. (17). For selected stages along the cascade reaction, solid lines show the analytical spectrum from the linear-noise approximation (normalized by the total power) and open circles show the normalized numerical spectrum calculated by averaging the periodograms of 750 realizations of the stochastic simulation algorithm and then normalizing by the total power (sum of all spectrum values × frequency resolution). The inset shows a realization of a time series of the number of $A$/$B$ molecules at the first stage ($n = 1$, red) and last stage ($n = 15$, black) of the cascade reaction, as obtained from the stochastic simulation algorithm. The unit for frequency $\omega$ is rad s$^{-1}$.

stochastic trajectories of these near-maximum quality NIO, as produced by the stochastic simulation algorithm, give rise to oscillations in the time series data which are not easily discernible by the naked eye. In other words, even though the oscillation is present, the noise is so large that it masks the former. In this section we show that for certain classes of chemical systems, the quality of stable node NIO considerably improves with the number of interacting species, eventually leading to pronounced oscillations in the time series data.

Consider the following reaction scheme:

$$\begin{aligned}
&\oslash \xrightarrow{k_0} A_1,\\
&2A_1 + B_1 \xrightarrow{k_1} 3A_1, \quad A_1 \xrightarrow{k_2} B_1,\\
&A_1 \xrightarrow{k_3} A_2,\\
&2A_2 + B_2 \xrightarrow{k_1} 3A_2, \quad A_2 \xrightarrow{k_2} B_2,\\
&A_2 \xrightarrow{k_3} A_3,\\
&\cdots\cdots\\
&2A_N + B_N \xrightarrow{k_1} 3A_N, \quad A_N \xrightarrow{k_2} B_N,\\
&A_N \xrightarrow{k_3} \oslash.
\end{aligned} \tag{48}$$

This describes a chain of $N$ downstream-connected Brusselator modules, and was first introduced by Shibata[40] (a similar model has been studied by means of deterministic rate equations by Tyson[28]) and further investigated by Ramaswamy and Sbalzarini.[41]

The cascade is composed of a chain of similar modules connected by an irreversible reaction. Steady-state conditions imply that the influx into a given module equals the outflux from this module to the next. Hence we have the condition $k_3[A_i]^* = k_0$ for $i \in \{1, N\}$, where $[A_i]^*$ is the steady-state concentration of species $A_i$. At all stages, the steady-state concentrations are the same, i.e., $[A_i]^* = [A_1]^*$; $[B_i]^* = [B_1]^*$ for all $i$. However, the dynamics of the fluctuations at each stage are very different; for example, Ramaswamy and Sbalzarini reported a downstream amplification of stable focus NIO.[41] Here we investigate whether this process also leads to a downstream improvement of the quality of stable node NIO.

Figure 13 shows the variation in the normalized power spectra (from the stochastic simulation algorithm and the linear-noise approximation) of $A$ and $B$ molecule fluctuations at different stages along a cascade chain of $N = 15$ Brusselators. At every stage of the cascade, the eigenvalues of the Jacobian of the deterministic rate equations describing this system are $-30$ and $-50$ (in units of s$^{-1}$) and hence the steady state is a stable node. Note how the quality of the stable node NIO improves as it is processed by successive stages, finally leading to remarkably large NIO (insets). The agreement between the spectra obtained from simulations and the linear-noise approximation is generally good, although some deviations can be discerned in the final stage. The drastic improvement in quality is evident for both species (see insets of Fig. 13; in Fig. 14 we also show a plot of the quality of the NIO in species A versus the cascade stage); this improvement in NIO quality is particularly spectacular for species $B$ since in this case in the first stage there is not even a stable node NIO and yet pronounced stable node NIO ensues at the final stage. Hence it is clear by this example that certain systems with more than 2 interacting species can lead to very high quality stable node NIO.

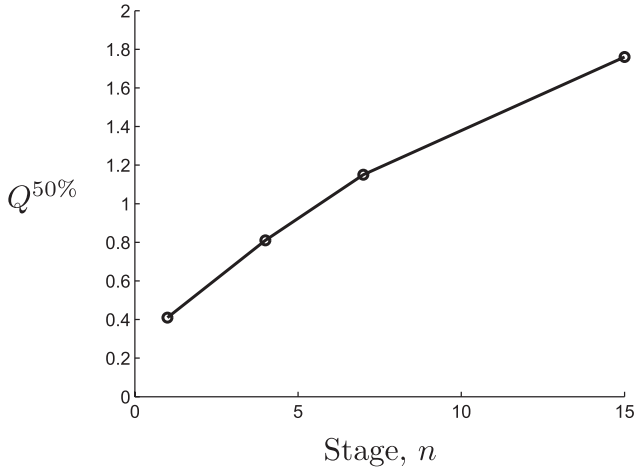


FIG. 14. Plot of the quality of the spectrum of the number fluctuations of species $A$ versus the stage of the cascade Brusselator reaction system. The quality is calculated using the theoretical linear noise approximation spectra shown in Fig. 13(a). Note that the quality of the NIO increases as the noisy oscillatory signal makes its way downstream through the cascade.

Because each stage of the cascade is identical in the rate constants, the dramatic increase in the NIO quality seen along the cascade can be understood as a resonance resulting from the action of a weak oscillator feeding back its output spectrum to itself, which therefore further excites the natural frequency. There are many developments which could be made to the model which are worthy of further investigation. In particular, it would be of interest to study the effect on NIO when there is variability in the cascade modules, and also to look at the effect of other forms of coupling, e.g., bi-directional coupling between stages or coupling stage $N$ to stage 1 and forming a cyclical reaction system.

## VII. EXTERNAL VERSUS INTERNAL NOISE INDUCED STABLE NODE OSCILLATIONS

In our investigation of internal noise NIO in exemplary biochemical systems, we observed two counter-intuitive properties: (i) for all of the reaction schemes, it was not possible to have NIO in both species within the stable node region; (ii) for the trimerization reaction, the maximum quality is attained at a point in parameter space within the stable node region and not the stable focus region. Since in Sec. III we established that stable node NIO are of the noise dependent type, it is a natural step to question whether the particular constraints placed on the diffusion matrix are fundamental in generating these counter-intuitive properties.

For a two-species system, the diffusion matrix $\mathbf{D}$ (describing either internal or external noise) can be written in the form,

$$\mathbf{D} = \begin{pmatrix} c_1 & c_2 \\ c_2 & c_3 \end{pmatrix} = \sigma_m \begin{pmatrix} \sigma_r^{-1/2} & \sigma_c \\ \sigma_c & \sigma_r^{1/2} \end{pmatrix},$$

where $\sigma_m = \sqrt{c_1 c_3}$, $\sigma_r = \frac{c_3}{c_1}$, $\sigma_c = \frac{c_2}{\sqrt{c_1 c_3}}$. The parameter $\sigma_m$ only scales the fluctuation spectrum in power ($y$-axis) and has no effect on the frequency composition of the spectrum. The other parameters satisfy the positive semi-definite requirement of $\mathbf{D}$ when $\sigma_r \in (0, \infty)$ and $\sigma_c \in [-1, 1]$.

In biochemical systems with internal noise, as described by the linear noise approximation, the diffusion and Jacobian matrices are in general intimately and non-trivially linked by their dependence on the rate constants (see Eqs. (7) and (8)). This coupling means that it is impossible to vary the parameters $\sigma_r$ and $\sigma_c$ independently of the underlying form of system stability. However, it is possible to uncouple these matrices and therefore directly study the importance of the precise form of the noise by reframing the biochemical model as one in which internal noise is negligible but external noise is significant. The details of an approach for introducing external noise for the trimerization reaction are given in Appendix E. The starting point is to assume that external noise sources introduce stochasticity in the rate constants, i.e., $\widetilde{k}_i(t) = k_i(1 + \epsilon\, \widetilde{\eta}_i(t))$, where $\epsilon$ is a small parameter and $\widetilde{\eta}_i(t)$ is Gaussian white noise. This results in an alternative linear stochastic differential equation for the concentration fluctuations (cf. Eq. (6)) given by

$$d\vec{\xi}^{\,e}(t) = \mathbf{J}\vec{\xi}^{\,e}(t)\, dt + \mathbf{B}^e\, d\vec{W}(t), \tag{49}$$

where the superscript $e$ denotes external noise. The matrix $\mathbf{J}$ is the same as for internal noise, but in the external noise case the diffusion matrix $\mathbf{D}^e = \mathbf{B}^e.(\mathbf{B}^e)^T$ can be changed independently of $\mathbf{J}$ by changing the external noise parameters (see Appendix E).

For the simple trimerization reaction, the internal noise forces the constants to take values: $\sigma_r = 1/4$ and $\sigma_c = -1/4$. In contrast, for external noise these constants can take any value provided they satisfy the positive semi-definite constraints mentioned earlier. In Fig. 15(a) we show the existence of NIO obtained from external noise for four different values of $\sigma_c$, and with $\sigma_r$ fixed to unity. Note that for internal noise stable node NIO were only possible in one species (see Fig. 11(a)) but for external noise it is possible to obtain NIO in both species in the stable node regime (region 5 for the case $\sigma_c = +0.99$).

With internal noise we found that the quality at a point in the stable node regime ($Q^{99\%}_{node} \approx 2.7$ when $\Lambda \approx 0.053$) is larger than in the focus regime ($Q^{99\%}_{focus} \approx 1.6$ when $\Lambda = 0.13$, see Fig. 11(b)). In Fig. 15(b) we show the variation of $Q^{99\%}_{node}$ and $Q^{99\%}_{focus}$ as a function of the noise coupling parameter $\sigma_c$ when $\sigma_r$ is fixed to the same value as for the internal noise ($\sigma_r = 1/4$). Note that when $\sigma_c < -0.8$, $Q^{99\%}_{focus} > Q^{99\%}_{node}$, indicating that at this level of external noise coupling the quality of stable focus NIO is better than stable node NIO, a case opposite to that observed for the reaction stimulated by internal noise. Hence it is clear that the counter-intuitive properties of stable node NIO as induced by internal noise stem from the special form of the diffusion matrix enforced by the linear-noise approximation. It is also interesting that this implies that the origin of noise plays a significant role in determining the properties of NIO. For example, for both the node and focus points, increasing positive noise coupling is observed to dramatically weaken and ultimately destroy the NIO. For the focus point, when $\sigma_c > -0.1$ the NIO are so weak that the power spectrum peak is all-but destroyed and the $Q^{99\%}$ value is undefined; the NIO disappear altogether for $\sigma_c \geq +0.1$. Interestingly, for the

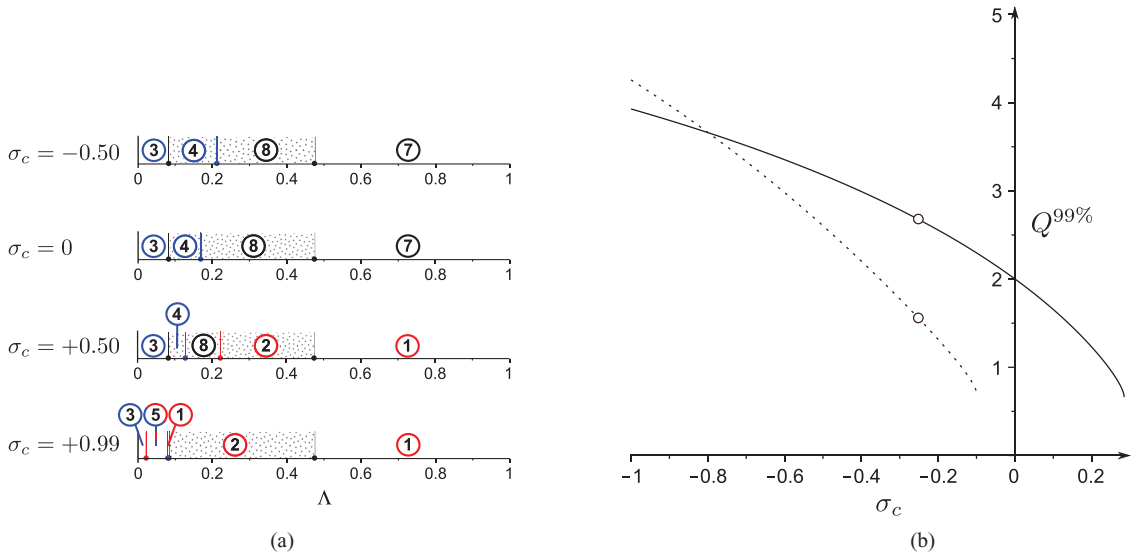


FIG. 15. Properties of NIO stimulated by external noise in the trimerization reaction. (a) Existence of external noise NIO as a function of the noise coupling strength parameter $\sigma_c$ with $\sigma_R$ held constant and equal to unity. When $\sigma_c \leq 0$ there are NIO only in species $B$, with similar behaviour as for internal noise (see Fig. 11(a)). For larger, positive, noise coupling $\sigma_c = +0.50$, NIO in $A$ become possible (region ①); for very large noise coupling $\sigma_c = +0.99$ it is possible to have NIO in both $A$ and $B$ (region ⑤). (b) Quality of external noise NIO as a function of the noise coupling strength parameter $\sigma_c$ with $\sigma_R$ held constant and equal to 1/4. The solid line is for the stable node point, $\Lambda \approx 0.053$, and the dotted line is for the stable focus point, $\Lambda = 0.13$. The open circles here correspond directly to the open circles in Fig. 11(b) as they indicate the external noise characteristics that exactly match the internal noise case. Note that when $\sigma_c < -0.8$ the quality is higher in the focus regime, i.e., opposite to that observed for internal noise NIO. Note also that the quality factor $Q^{99\%}$ is calculated as the peak frequency divided by the difference of the two frequencies at which the spectrum achieves 99% of its maximum power.

node point, NIO with defined $Q^{99\%}$ exist for noise coupling values as large as $\sigma_c \approx +0.3$.

We note in passing that an example of a stable node giving rise to NIO has recently been reported by Qian who showed that for a particular numerical choice of the Jacobian and diffusion matrices, one can obtain a peak in the power spectrum for a stable node (see Fig. 3 of Ref. 42). This example falls within the general category of stable node NIO stimulated by external noise since the Jacobian and diffusion matrices are not constrained by means of the linear-noise approximation. Our work in the present article goes further than[42] by developing a general theory of stable node NIO in the presence of both internal and external noise and studying the quality of these noisy oscillations in realistic biochemical models.

## VIII. DISCUSSION AND CONCLUSION

In this article, we have shown that NIO can be induced by internal noise in biochemical systems characterized by deterministic stable node steady states. This phenomenon goes beyond the conventional well-known case in which NIO are induced by noise for systems with a deterministic focus steady state since stable nodes do not possess an intrinsic frequency which can be stimulated by white noise. Rather the frequency of stable node NIO is determined by the time scales characterizing the non-oscillatory decay of perturbations in stable nodes; in particular for two species systems, the frequency is bounded from above by the geometric mean of the two real eigenvalues of the Jacobian. Although our results are presented in the context of biochemical reactions, the same can be envisaged to occur in other scenarios such as predator-prey systems subject to demographic fluctuations[43] and chemostats subject to fluctuations in nutrient and biomass levels.[44]

These stable node NIO possess properties which are counter-intuitive. For example, for deterministic oscillatory systems and for stable focus NIO close to the Hopf bifurcation oscillations are present in all interacting species, but for stable node NIO we find that this is not generally the case. We note that for internal noise, the linear-noise approximation enforces a complicated dependence of the diffusion matrix on the elements of the Jacobian matrix and on the stoichiometric matrix and that this could be the origin of the counter-intuitive property delineated above. This line of thought is suggested by the fact that if the elements of the diffusion matrix could be freely chosen then the counter-intuitive property can be eliminated by appropriate choices (Sec. VII). This indeed turns out to be the fundamental reason why stable node NIO stimulated by external noise may have different properties than those stimulated by internal noise since the former (unlike the latter) is characterized by a diffusion matrix which can take any values, provided the matrix is positive semi-definite.

It is also the case that one would expect NIO for stable foci to be of better quality than stable node NIO because in the former there exists a clear internal frequency which can be stimulated by white noise while in the latter there is not. However, we found that this is not generally the case: there are stable foci regions in parameter space where there are no NIO (region 8 in Figs. 4(a), 7(a), and 11(a)) whereas there are stable node regions where NIO are present (regions 1 and 3 in Figs. 4(a), 7(a), and 11(a)). For the trimerization reaction we found that the NIO quality maximized in the node region and subsequently decreased as one approached the node-focus borderline (Fig. 11(b)). Furthermore as we saw for the cascade reaction system of Sec. VI, the quality of stable node

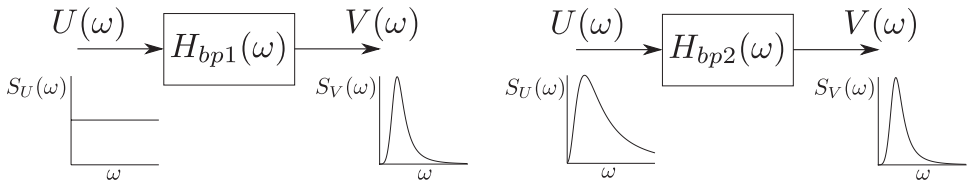


FIG. 16. From LTI theory, the filtering action of the bandpass filter $H$ on an input stationary process with spectrum $S_U(\omega)$ results in an output stationary process with spectrum $S_V(\omega)$. (a) Bandpass filter $H_{bp1}$ with white noise input, (b) A different bandpass filter $H_{bp2}$ whose input process has a spectrum which matches that of a selected variable in one of the parameterized biochemical models. For an output spectrum $S_V(\omega)$ with the same quality in (a) and (b), the required bandpass filter parameter $Q_{bp2} < Q_{bp1}$, i.e., the filter in (b) requires less filtering to achieve an optimal output than the filter in (a) since the input to the filter in (b) is of higher quality than the input to the filter in (a).

NIO increases as the noisy signal makes its way downstream through the network eventually leading to massive NIO, similar to those previously observed for stable foci.[16]

We have also shown that stable node NIO do occur for chemical systems with mean molecule numbers ranging from the order of one to a few thousand (see Figs. 6 and 13), i.e., the physiologically relevant range.[9] Furthermore, we have identified two chemical systems composed of at most bimolecular reactions and each involving merely two species, in which noise induces oscillations; this is in contrast to the well-known deterministic result that at least three species are needed to obtain limit cycle oscillations from elementary reaction models.[7,45] It is, however, the case that oscillations for two species systems are very noisy and their quality improves considerably as the number of interacting species increases.

We conclude from our study that noise can induce oscillations over larger regions of parameter space and for simpler chemical systems than currently thought, hence further amplifying the current trend of thought that noise plays a constructive and essential role in cellular regulation.[46,47]

## ACKNOWLEDGMENTS

D.L.K.T. and R.G. acknowledge support by SULSA (Scottish Universities Life Science Alliance).

## APPENDIX A: EXISTENCE OF NIO FOR STABILITY DOMINATED & NOISE DEPENDENT CASES

In the large $\omega$ limit, $S_i(\omega)$ monotonically decreases as $\omega^{-2}$. In the opposite limit of small $\omega$, we have

$$S_i(\omega) = \frac{1}{p}\alpha_i + \frac{1}{p}\left(\beta_i - \frac{\alpha_i\, q}{p}\right)\omega^2 + O(\omega^4).$$

A peak in the power spectrum will then exist if the spectrum increases for small $\omega$, i.e., if the $\omega^2$ term above is positive. As shown in Sec. III, the parameters $p$, $\alpha_i$, and $\beta_i$ are positive. For a stability dominated NIO, $q < 0$ and hence a peak always exists. For noise dependent NIO, $q \geq 0$ and hence a peak only exists if $\beta_i > \alpha_i q/p$.

For both cases, it can be further shown that the peak power in $S_i(\omega)$ occurs at a frequency lying between the peak frequencies of the two sub-spectra. The proof is as follows. Let the $S_i^\alpha$ and $S_i^\beta$ subspectra have peaks at the frequencies $\hat{\omega}_{S^\alpha}$ and $\hat{\omega}_{S^\beta}$, respectively. Taylor expanding $S_i(\omega)$ at these two frequencies, one finds that the slope of $S_i(\omega)$ at $\omega = \hat{\omega}_{S^\alpha}$ is $>0$, and the slope at $\omega = \hat{\omega}_{S^\beta}$ is $<0$. Since there can only be a single peak in the spectrum of a two species system, it follows that the peak power in $S_i(\omega)$ is in the range $(\hat{\omega}_{S^\alpha}, \hat{\omega}_{S^\beta})$.

## APPENDIX B: VALIDATION OF THE $Q^{99\%}$ MEASURE USING LINEAR FILTER THEORY

In this section we validate the $Q^{99\%}$ measure used to determine the quality for weak stable node oscillations in the main text. The underlying idea is as follows. Consider a filter whose input signal has the same power spectrum as a selected variable in one of the biochemical models studied in Sec. V. Now say that the output of the filter should be such that its power spectrum has some chosen optimal quality factor. It then follows that the lower the quality of the input signal, the larger the degree of filtering needed to be performed by the filter. Hence if the $Q^{99\%}$ measure is reliable then we expect an inverse relationship between it and the degree of filtering. In what follows we now flesh out these ideas using the theory of linear time invariant (LTI) filters.

If a stable LTI system with gain function $H$ takes as its input ($U$) a stationary process with spectrum $S_U(\omega)$, the output $V$ is also a stationary process with power spectrum given by[48]

$$S_V(\omega) = H^2(\omega) S_U(\omega).$$

Figure 16(a) shows an illustrative example where the input is stationary white noise and $H$ is the gain function of a simple bandpass filter, given by

$$H_{bp1}(\omega) = \left| \frac{\hat{\omega}_{bp1}\,\omega}{-Q_{bp1}\,\omega^2 + i\,\hat{\omega}_{bp1}\,\omega + \hat{\omega}_{bp1}^2\,Q_{bp1}} \right|.$$

With this system, the output spectrum $S_V(\omega)$ has a peak at $\omega = \hat{\omega}_{bp1}$ and (conventional) $Q$-factor given by $Q_V^{50\%} = Q_{bp1}$. Note that this $Q$-factor is a measure of the degree of filtering that the filter performs.

We validated the $Q^{99\%}$ quality measure of stable node oscillations by considering another LTI bandpass filter system in which the spectrum of the input process is the fluctuation spectrum of a particular species in one of the biochemical models (Fig. 16(b)). Specifically, for each of the three biochemical systems evaluated at the parameters in Figs. 5, 8, 9, and 12, we considered the problem of obtaining an output quality $Q_V^{50\%} = 1$ by selecting an appropriate value of $Q_{bp2}$

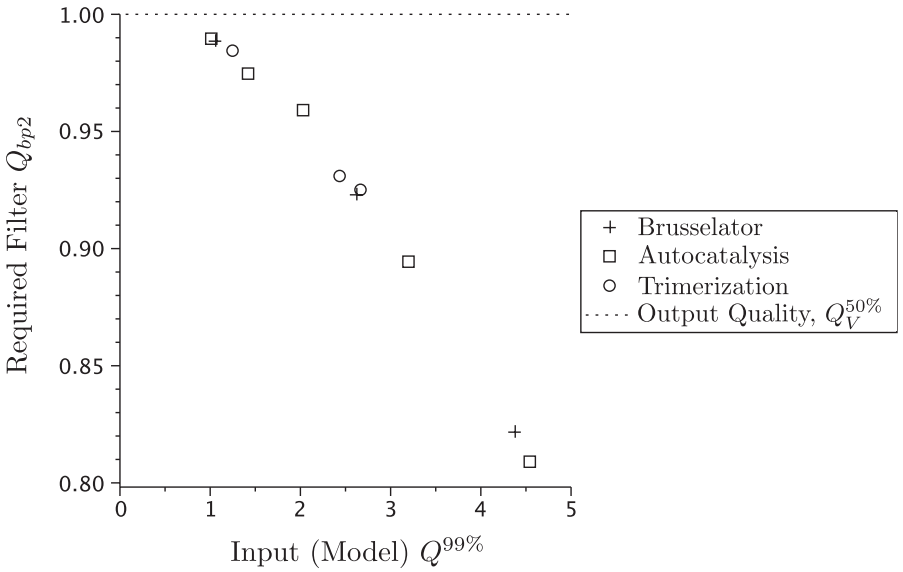


FIG. 17. With the setup as shown in Fig. 16(b) and inputs with spectra from the parameterized biochemical models (Figs. 5, 8, 9, and 12), the required additional filter quality $Q_{bp2}$ was determined for a "system" (output) quality of $Q_V^{50\%} = 1$. The figure shows that a biochemical species whose spectrum has a low value of $Q^{99\%}$ (here the input (model) $Q^{99\%}$) requires a greater degree of filtering (larger $Q_{bp2}$ value) for an output $Q_V^{50\%} = 1$. This inverse relationship validates the use of $Q^{99\%}$.

for a bandpass filter described by

$$H_{bp2}(\omega) = \left| \frac{\hat{\omega}_U\, \omega}{-Q_{bp2}\, \omega^2 + i\, \hat{\omega}_U\, \omega + \hat{\omega}_U^2\, Q_{bp2}} \right|.$$

Note that here we tune the parameter $\hat{\omega}_{bp2}$ to the value of the peak frequency of the particular input fluctuation spectrum, $\hat{\omega}_U$, so that the bandpass filter works constructively with the input to create a higher quality output. If the $Q^{99\%}$ measure is valid then we would expect that for input spectra with high $Q^{99\%}$ values, lower values of $Q_{bp2}$ would be required to obtain $Q_V^{50\%} = 1$. This was indeed found to be the case, as shown in Fig. 17, which validates the use of $Q^{99\%}$.

## APPENDIX C: POWER SPECTRUM ESTIMATES FROM THE STOCHASTIC SIMULATION ALGORITHM

From a single realization $r$ of the stochastic simulation algorithm, the number of molecules $n^r(t)$ of a particular species over some time interval $T$ was regularly sampled at $L$ discrete points separated by $\Delta t$ (such that $(L-1)\Delta t = T$).

Using the notation $n_l^r \equiv n^r(l\Delta t), l \in [0, L-1]$, the fluctuation in numbers of molecules about the mean is $\hat{n}_l^r = n_l^r - \sum_{j=0}^{L-1} n_j^r$. The discrete Fourier transform of $\hat{n}^r$, which we denote $N^r$, was calculated by

$$N_k^r = \sum_{l=0}^{L-1} \hat{n}_l^r\, e^{-2\pi i l k/L}, \quad k \in [0, L-1]. \tag{C1}$$

From this, the one-sided periodogram estimate, $P^r$, of the number fluctuation power spectrum from realization $r$ is defined as[49]

$$P_k^r = \frac{1}{L^2} \begin{cases} \left|N_k^r\right|^2 & k = 0, \frac{L}{2} \\ \left|N_k^r\right|^2 + \left|N_{L-k}^r\right|^2 & k \in \left[1, \frac{L}{2} - 1\right] \end{cases}. \tag{C2}$$

The $\frac{L}{2} + 1$ frequencies $\omega_k$ over which $P^r$ is defined span the frequency range $[0, \omega_{Nyq}]$ where $\omega_{Nyq}$ is the Nyquist rate, $\omega_{Nyq} = \frac{\pi}{\Delta t}$ rad s$^{-1}$. The frequency interval $\Delta\omega$ between $\omega_k$ and $\omega_{k+1}$ is $\Delta\omega = \frac{2\pi}{L\Delta t}$ rad s$^{-1}$.

Since $\hat{n}_l^r$ has zero mean, $P_0^r = 0$. The remaining $\frac{L}{2}$ periodogram values are normalized in Eq. (C2) such that $\sum_{k=1}^{L/2} P_k^r = \sigma_{\hat{n}^r}^2$ where $\sigma_{\hat{n}^r}^2$ is the sample variance of $\hat{n}^r$, i.e., $\sigma_{\hat{n}^r}^2 = \frac{1}{L}\sum_{l=0}^{L-1} (\hat{n}_l^r)^2$. For comparison with the spectrum from the linear-noise approximation, Eq. (9), which is truly a power spectral density, we desire that the integral and not the sum of the numerical spectral density over these $\frac{L}{2}$ frequencies is equal to $\sigma_{\hat{n}^r}^2$.

The value of $P^r$ at frequency $\omega_k = \frac{2\pi k}{L\Delta t}$ represents some average of the power within the frequency bin $\omega_k \pm \frac{1}{2}\Delta\omega$.[49] By assuming that the power in a frequency bin $\omega_k \pm \frac{1}{2}\Delta\omega$ is uniformly distributed within that bin, the integral-normalized form of the power spectral density over the frequency range $(\omega_1 - \frac{1}{2}\Delta\omega, \omega_{\frac{L}{2}} + \frac{1}{2}\Delta\omega)$ is given by

$$S^r\left(\omega_k \pm \frac{1}{2}\Delta\omega\right) = \frac{1}{\Delta\omega} P_k^r, \quad k \in \left[1, \frac{L}{2}\right]. \tag{C3}$$

For display purposes in Figs. 5, 8, 9, and 12, we represent the power spectral density estimate over the frequency bin $\omega_k \pm \frac{1}{2}\Delta\omega$ by a single point of value $S^r(\omega_k \pm \frac{1}{2}\Delta\omega)$ at $\omega_k$. We refer to this as $S_k^r$.

Finally, since the variance of the estimate $S^r$ at a single frequency $k$ from the periodogram method is known to be high, we obtain the final numerical power spectral density estimate by averaging $S^r$ over $R$ realizations, i.e.,

$$S_k = \frac{1}{R}\sum_{r=1}^{R} S_k^r. \tag{C4}$$

## APPENDIX D: ESTIMATION OF $Q^{50\%}$ VALUES FROM THE NUMERICAL POWER SPECTRUM

For each of the numerical power spectra $S^{SSA}$ from the stochastic simulation algorithm shown in Fig. 6(a), the $Q^{50\%}$ was determined as follows. First we fit the numerical power spectra using a function of the form,

$$S^{fit} = \frac{\alpha + \beta\omega^2}{p + q\omega^2 + \omega^4}.$$

We then use the parameterized function to find $\hat{\omega}$ (the frequency at which the power maximizes) and $\Delta\omega$ (the difference of the two frequencies at which the power is half maximum) analytically, from which we finally obtain $Q^{50\%} = \hat{\omega}/\Delta\omega$. To determine the parameters of $S^{fit}$, the MATLAB optimization toolbox function fminsearch was used to perform an unconstrained parameter search which minimized the Euclidean norm between the data and the fitted function, i.e., $C = \sqrt{\sum_{k=1}^{L/2}(S_k^{fit} - S_k^{SSA})^2}$.

## APPENDIX E: TRIMERIZATION REACTION WITH EXTERNAL NOISE

Consider the trimerization reaction scheme discussed in Sec. V. When there is no noise of any form, the deterministic rate equations for the concentrations are given by

$$\partial_t \phi_A(t) = k_0 - 2k_1\phi_A^2(t) - k_2\phi_A(t)\phi_B(t), \tag{E1}$$

$$\partial_t \phi_B(t) = k_1\phi_A^2(t) - k_2\phi_A(t)\phi_B(t). \tag{E2}$$

Now consider the case when there is some external noise present in the system. One method of representing external noise is by allowing the rate constants to be stochastic.[50] White Gaussian noise processes $\widetilde{\eta}_i(t)$ are added to the rate constants and scaled by a small parameter, $\epsilon$, so that the new stochastic rate constants read

$$\widetilde{k}_i(t) = k_i(1 + \epsilon\,\widetilde{\eta}_i(t)), \tag{E3}$$

where the tilde is used throughout to denote a random variable. It follows that the dynamics in the presence of external noise is described by the stochastic rate equations:

$$\partial_t \widetilde{\phi}_A(t) = \widetilde{k}_0(t) - 2\widetilde{k}_1(t)\widetilde{\phi}_A{}^2(t) - \widetilde{k}_2(t)\widetilde{\phi}_A(t)\widetilde{\phi}_B(t), \tag{E4}$$

$$\partial_t \widetilde{\phi}_B(t) = \widetilde{k}_1(t)\widetilde{\phi}_A{}^2(t) - \widetilde{k}_2(t)\widetilde{\phi}_A(t)\widetilde{\phi}_B(t). \tag{E5}$$

We solve these equations by making the ansatz,

$$\widetilde{\phi}_i(t) = \phi_i^* + \epsilon\,\widetilde{\xi}_i^e(t), \tag{E6}$$

where $\phi_A^* = \sqrt{\frac{k_0}{3k_1}}$ and $\phi_B^* = \frac{k_1}{k_2}\sqrt{\frac{k_0}{3k_1}}$ are the steady-state solutions of the deterministic rate equations Eqs. (E1) and (E2) in the absence of any noise and $\epsilon\,\widetilde{\xi}_i^e(t)$ represents the stochastic contribution about $\phi_A^*$, $\phi_B^*$. Collecting terms of order $\epsilon$ we obtain

$$\partial_t \begin{bmatrix} \widetilde{\xi}_A^e(t) \\ \widetilde{\xi}_B^e(t) \end{bmatrix} = \sqrt{\frac{k_0}{3k_1}} \begin{bmatrix} -5k_1 & -k_2 \\ k_1 & -k_2 \end{bmatrix} \begin{bmatrix} \widetilde{\xi}_A^e(t) \\ \widetilde{\xi}_B^e(t) \end{bmatrix} + \frac{k_0}{3} \begin{bmatrix} 3 & -2 & -1 \\ 0 & 1 & -1 \end{bmatrix} \begin{bmatrix} \widetilde{\eta}_0(t) \\ \widetilde{\eta}_1(t) \\ \widetilde{\eta}_2(t) \end{bmatrix},$$

or

$$\partial_t \begin{bmatrix} \widetilde{\xi}_A^e(t) \\ \widetilde{\xi}_B^e(t) \end{bmatrix} = \sqrt{\frac{k_0}{3k_1}} \begin{bmatrix} -5k_1 & -k_2 \\ k_1 & -k_2 \end{bmatrix} \begin{bmatrix} \widetilde{\xi}_A^e(t) \\ \widetilde{\xi}_B^e(t) \end{bmatrix} + \begin{bmatrix} \widetilde{w}_A(t) \\ \widetilde{w}_B(t) \end{bmatrix},$$

$$\widetilde{w}_A(t) = \frac{k_0}{3}\left(3\widetilde{\eta}_0(t) - 2\widetilde{\eta}_1(t) - \widetilde{\eta}_2(t)\right),$$

$$\widetilde{w}_B(t) = \frac{k_0}{3}\left(\widetilde{\eta}_1(t) - \widetilde{\eta}_2(t)\right).$$

The symmetric positive semi-definite external noise diffusion matrix $\mathbf{D}^e$ is defined by

$$\langle \widetilde{w}_i(t)\widetilde{w}_j(t')\rangle = D^e_{i,j}\delta(t - t'),\ i, j = 1, 2,$$

where in the above notation $w_1 = w_A$ and $w_2 = w_B$. We obtain this matrix by writing the $3 \times 3$ symmetric positive semi-definite covariance matrix $\mathbf{C}$ for the external noise $\eta_0$, $\eta_1$, and $\eta_2$ as

$$\langle \widetilde{\eta}_i(t)\widetilde{\eta}_j(t')\rangle = C_{i+1,j+1}\delta(t - t'),\ i, j = 0, 1, 2.$$

As an example, the term $D^e_{1,1} = \langle \widetilde{w}_A(t)\widetilde{w}_A(t')\rangle$ is given by

$$D^e_{1,1} = \langle \widetilde{w}_A(t)\widetilde{w}_A(t')\rangle,$$

$$= \frac{k_0^2}{9}(9C_{1,1} - 12C_{1,2} - 6C_{1,3} + 4C_{2,2} + 4C_{2,3} + C_{3,3}).$$

Writing the matrix $\mathbf{D}^e$ in the form

$$\mathbf{D}^e = \sigma_m \begin{pmatrix} \sigma_r^{-1/2} & \sigma_c \\ \sigma_c & \sigma_r^{1/2} \end{pmatrix},$$

we find that the noise parameters $\sigma_r$ and $\sigma_c$ are given as functions only of the $C_{i,i}$ (but in a combination which is specific for the trimerization reaction scheme):

$$\sigma_r = \frac{C_{2,2} - 2\,C_{2,3} + C_{3,3}}{9\,C_{1,1} - 12\,C_{1,2} - 6\,C_{1,3} + 4\,C_{2,2} + 4\,C_{2,3} + C_{3,3}},$$

$$\sigma_c = \frac{3\,C_{1,2} - 3\,C_{1,3} - 2\,C_{2,2} + C_{2,3} + C_{3,3}}{\sqrt{(9\,C_{1,1} - 12\,C_{1,2} - 6\,C_{1,3} + 4\,C_{2,2} + 4\,C_{2,3} + C_{3,3})(C_{2,2} - 2\,C_{2,3} + C_{3,3})}}.$$

Varying the external noise parameters, $C_{i,i}$, allows a large range of possible $\sigma_r$, $\sigma_c$. Given no prior information about the external noise, we might propose that noise in the input reaction parameter $k_0$ is uncorrelated with the noise in the other parameters, i.e., $C_{1,2} = C_{1,3} = C_{2,1} = C_{3,1} = 0$, but that the other parameters are only constrained so far as to give a positive semi-definite **C** matrix. We were able to find noise matrices to satisfy these criteria for all of the $\sigma_r$, $\sigma_c$ values used in the investigation of external noise in Fig. 15.

The power spectra of the new stochastic differential equation can be calculated using Eq. (10) in the main text. NIO due to external noise are obtained whenever the spectrum displays a maximum at some peak frequency.


[1] A. Goldbeter, *Biochemical Oscillations and Cellular Rhythms: The Molecular Bases of Periodic and Chaotic Behaviour* (Cambridge University Press, 1996).
[2] R. E. Dolmetsch, K. Xu, and R. S. Lewis, Nature (London) **392**, 933 (1998).
[3] P. Richard, B. Teusink, M. B. Hemker, K. van Dam, and H. V. Westerhoff, Yeast **12**, 731 (1996).
[4] J. C. Dunlap, Cell **96**, 271 (1999).
[5] J. D. Murray, *Mathematical Biology: I. An Introduction* (Springer, 2007).
[6] B. Novák and J. J. Tyson, Nat. Rev. Mol. Cell. Biol. **9**, 981 (2008).
[7] T. Wilhelm and R. Heinrich, J. Math. Chem. **17**, 1 (1995).
[8] Y. Ishihama, T. Schmidt, J. Rappsilber, M. Mann, F. U. Hartl, M. J. Kerner, and D. Frishman, BMC Genomics **9**, 102 (2008).
[9] R. Grima and S. Schnell, Essays Biochem. **45**, 41 (2008).
[10] J. M. G. Vilar, H. Y. Kueh, N. Barkai, and S. Leibler, Proc. Natl. Acad. Sci. U.S.A. **99**, 5988 (2002).
[11] D. Gonze, J. Halloy, and A. Goldbeter, Proc. Natl. Acad. Sci. U.S.A. **99**, 673 (2002).
[12] D. B. Forger and C. S. Peskin, Proc. Natl. Acad. Sci. U.S.A. **102**, 321 (2005).
[13] H. Li, Z. Hou, and H. Xin, Phys. Rev. E **71**, 061916 (2005).
[14] D. T. Gillespie, J. Phys. Chem. **81**, 2340 (1977).
[15] N. G. van Kampen, *Stochastic Processes in Physics and Chemistry* (Elsevier, 2007).
[16] A. J. McKane, J. D. Nagy, T. J. Newman, and M. O. Stefanini, J. Stat. Phys. **128**, 165 (2007).
[17] T. Dauxois, F. Di Patti, D. Fanelli, and A. J. McKane, Phys. Rev. E **79**, 036112 (2009).
[18] R. Kuske, L. F. Gordillo, and P. Greenwood, J. Theor. Biol. **245**, 459 (2007).
[19] H. Qian and M. Qian, Phys. Rev. Lett. **84**, 2271 (2000).
[20] M. Scott, B. Ingalls, and M. Kærn, Chaos **16**, 026107 (2006).
[21] D. T. Gillespie, Annu. Rev. Phys. Chem. **58**, 35 (2007).
[22] C. W. Gardiner, *Handbook of Stochastic Methods for Physics, Chemistry and the Natural Sciences* (Springer, 2004).
[23] J. Elf and M. Ehrenberg, Genome Res. **13**, 2475 (2003).
[24] Note that a degenerate node could be of the star node type whereby the Jacobian has two independent eigenvectors and there is no curvature in the phase space trajectories. This is however a special case appearing when the Jacobian is diagonal and hence when the two species are non-interacting; the power spectrum Eq. (10) does not display a maximum in frequency for this case and hence no NIO either. Thus the only degenerate node case where NIO appear is where the Jacobian is not diagonal, i.e., the case of one independent eigenvector which is also characterized by curved trajectories, as discussed in the main text.
[25] K. L. Davis and M. R. Roussel, FEBS J. **273**, 84 (2006).
[26] I. Prigogine and R. Lefever, J. Chem. Phys. **48**, 1695 (1968).
[27] R. Lefever, G. Nicolis, and P. Borckmans, J. Chem. Soc., Faraday Trans. I **84**, 1013 (1988).
[28] J. J. Tyson, J. Chem. Phys. **58**, 3919 (1973).
[29] J. J. Tyson and J. C. Light, J. Chem. Phys. **59**, 4164 (1973).
[30] R. T. Pack, R. B. Walker, and B. K. Kendrick, J. Chem. Phys. **109**, 6714 (1998).
[31] R. T. Pack, R. B. Walker, and B. K. Kendrick, J. Chem. Phys. **109**, 6701 (1998).
[32] R. S. Berry, S. A. Rice, and J. Ross, *Physical and Chemical Kinetics* (Oxford University Press, 2002).
[33] P. Thomas, A. V. Straube, and R. Grima, J. Chem. Phys. **135**, 181103 (2011).
[34] P. Thomas, A. V. Straube, and R. Grima, BMC Syst. Biol. **6**, 39 (2012).
[35] G. B. Cook, P. Gray, D. G. Knapp, and S. K. Scott, J. Phys. Chem. **93**, 2749 (1989).
[36] N. Kellershohn and M. Laurent, Biophys. J. **81**, 2517 (2001).
[37] J. J. Tyson, Proc. Natl. Acad. Sci. U.S.A. **88**, 7328 (1991).
[38] C. Choudhary and M. Mann, Nat. Rev. Mol. Cell Biol. **11**, 427 (2010).
[39] M. Åkerfelt, R. I. Morimoto, and L. Sistonen, Nat. Rev. Mol. Cell Biol. **11**, 545 (2010).
[40] T. Shibata, Phys. Rev. E **69**, 056218 (2004).
[41] R. Ramaswamy and I. F. Sbalzarini, Sci. Rep. **1**, 154 (2011).
[42] H. Qian, Nonlinearity **24**, R19 (2011).
[43] A. J. McKane and T. J. Newman, Phys. Rev. Lett. **94**, 218102 (2005).
[44] F. Campillo, M. Joannides, and I. Larramendy-Valverde, Ecol. Modell. **222**, 2676 (2011).
[45] P. Hanusse, Comptes Rendus, Acad. Sci. Paris,(C) **274**, 1245 (1972).
[46] C. V. Rao, D. M. Wolf, and A. P. Arkin, Nature (London) **420**, 231 (2002).
[47] A. Eldar and M. B. Elowitz, Nature (London) **467**, 167 (2010).
[48] C. Chatfield, *The Analysis of Time Series: An Introduction* (Chapman and Hall/CRC, 2004).
[49] W. H. Press *et al.*, *Numerical Recipes in C: The Art of Scientific Scientific Computing* (Cambridge University Press, 1992).
[50] V. Shahrezaei, J. F. Ollivier, and P. S. Swain, Mol. Sys. Biol. **4**, 196 (2008).